Application and Analysis of Time Delayed Feedback Control on the Swift-Hohenberg Equation

als Masterarbeit vorgelegt von
Alexander Kraft

April 2014

institut für theoretische physik

Westfälische Wilhelms-Universität Münster

Contents

1 Motivation and Introduction of Concepts

Patterns often arise in technical applications or in nature, such as the formation of patterns on the skin of animals [Mur93], e.g., of giraffes, zerbras, fish, or as vegetation patterns [vHMSZ01]. In technical applications pattern formation can be applied, e.g., to form prestructures of semi–conductor wafers with pre–defined wave length, or to transmit information in optical systems [ABR99].

In order to describe pattern formation from the theoretical point of view, one develops models with the goal to reproduce and characterize the occurring patterns. In this thesis, we focus on pattern formation in the Swift–Hohenberg equation [SH77] (SHE). The SHE is an evolution equation for a real-valued order parameter that describes systems in the vicinity of a bifurcation in which a critical wave number k_c becomes unstable. The Swift–Hohenberg equation was first derived by J. Swift and P. C. Hohenberg to describe convection patterns which have been experimentally observed in the Rayleigh-Bénard system (Fig. 1.1). Since then, apart from hydro-

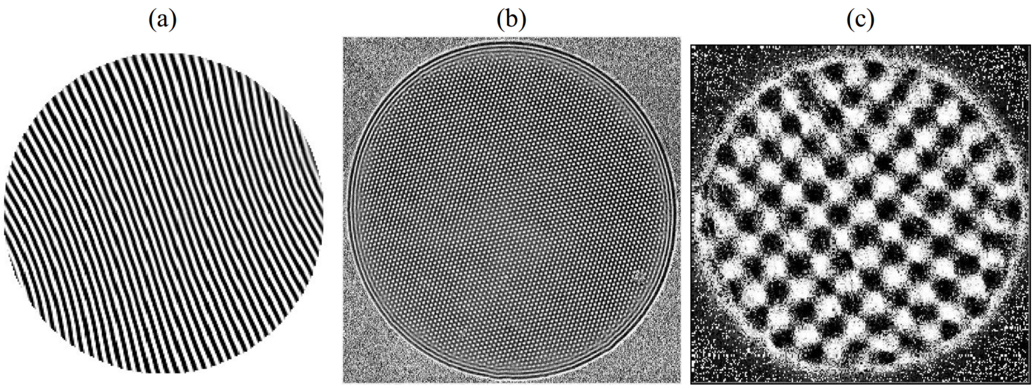

Figure 1.1: Experimental observation of convection patterns in the Rayleigh-Bénard system [BPA00]. From left to right: a) rolls, b) hexagons, c) squares.

dynamics, the Swift-Hohenberg equation has been used in a variety of problems, e.g., in nonlinear optics [LMN94], biology [LM99] and chemistry [SSM98]. We will analyze the properties and solutions of the Swift–Hohenberg equation in detail in chapter 2.

Depending on the context, certain system states can be more desirable than others and therefore one is interested in setting the system parameters accordingly, which can be a nontrivial task. Whereas parameters can be freely chosen in theory, in nature or experiment some parameters are fixed or can only be varied within certain limits. Therefore, in some cases, setting up the right parameter values to obtain a certain result can be impossible or can involve a disproportionate effort. Furthermore, it may be desirable to enforce a particular behaviour which is not intrinsic to the system. To solve these problems, an *external control mechanism* can be used.

In general, a control mechanism introduces a control–scheme–based contribution to components or parameters of the system in order to manipulate the system state. Since there is no general mechanism which is applicable to every type of system and which fulfills all requirements, various control mechanisms have been proposed and investigated. An overview of suitable control mechanisms for the control of chaos can be found in [SS08], whereas [MS06] provides an overview of control techniques in chemical systems.

In this thesis, we investigate the so–called *time delayed feedback* (TDF) *control* mechanism, also known as Pyragas control or autosynchronization, which was first proposed by Pyragas [Pyr92]. We aim to characterize its influence on the dynamical behaviour of spatially extended systems in chapters 3 and 4. Figure 1.2 illustrates the TDF mechanism for a general dynamical system. Let $\boldsymbol{x}$ denote the state of a system with input $\boldsymbol{h}(t)$ and output $\boldsymbol{s}(\boldsymbol{x}, t)$. The system output $\boldsymbol{s}(\boldsymbol{x}, t)$ as a function of system state $\boldsymbol{x}$ is re–injected into the system as follows: The difference between the system output at times t and $t - \tau$ is multiplied with a *coupling matrix* $\underline{\underline{K}}$ and is re–injected into the system. Thereby, the coupling matrix $\underline{\underline{K}}$ allows to couple different components of the state vector $\boldsymbol{x}$ within the feedback loop. The mechanism can be summarized as

$$\partial_t \boldsymbol{x} = \boldsymbol{F}[\boldsymbol{x}] + \underline{\underline{K}} \, (\boldsymbol{s}(\boldsymbol{x}, t) - \boldsymbol{s}(\boldsymbol{x}, t - \tau)), \tag{1.1}$$

where $\boldsymbol{F}[\boldsymbol{x}]$ describes the intrinsic dynamics of the dynamical system and τ denotes the *delay time*.

Time delayed feedback has been widely applied in experiments, especially but not only in the control of chaos, and has been extensively studied for nonlinear ordinary differential equations. Examples include the control of chaotic Taylor-Couette flow with TDF [LWP01], time-delay autosynchronization of the spatiotemporal dy-

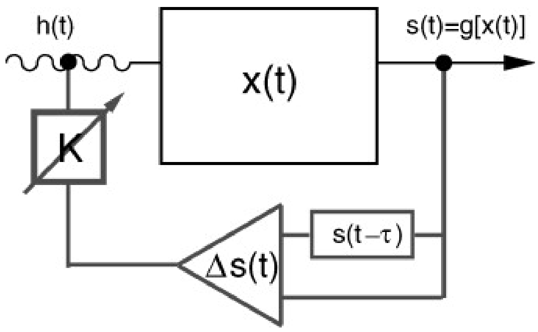

Figure 1.2: Setup of time–delayed feedback control [JBvL04] for a system with system state $\boldsymbol{x}$, input signal $\boldsymbol{h}(t)$ and output signal $\boldsymbol{s}(\boldsymbol{x}, t)$. The coupling matrix $\underline{\underline{K}}$ allows to couple different components of the system within the feedback loop.

namics in resonant tunneling diodes [UAJS03], or the self-stabilization of high-frequency oscillations in semiconductor superlattices by time-delay autosynchronization [SAJ$^+$03].

In recent years, a new area of research has emerged which analyzes the impact of TDF in spatially extended systems, both from the point of view of control and for systems in which delayed feedback naturally arises, e.g., for systems in which the evolution of a quantity depends on its history. Examples include the spontaneous motion of cavity solitons induced by delayed feedback in nonlinear optics [TVPT09, PVG$^+$13], TDF control of localized structures in a reaction–diffusion system [Gur13], dynamics of Turing structures in the Lengyel–Epstein model with TDF [ITSO13], delay–driven irregular spatiotemporal patterns in a predator–prey model for plankton in biology [TZ13], control of spatiotemporal patterns in the Gray–Scott model [KBHS09], TDF control in excitable media [SSD09], and the investigations of pattern transitions due to TDF [LH07].

The suggested control scheme (1.1) has the following advantages and problems to solve:

Advantages:

- This control mechanism is typically easy to set up from the experimental point of view, and requires little to no knowledge of the underlying system processes.

- The stability of solutions can be changed via a suitable choice of TDF control parameters.

- The control scheme is non–invasive, which means the set of steady state solutions does not change, since the control term vanishes once the final state is reached. The same holds for periodic solutions, if the delay time τ is a multiple of the period of the periodic orbit.

Disadvantages and Problems to Solve:

- A theoretical description requires the analysis of delay differential equations.
- The dynamics takes place in an infinite dimensional phase space [Hal93], even for ordinary differerential equations.

Within this thesis, we provide a general analysis for systems subjected to linear TDF, and then consider the Swift–Hohenberg equation with TDF, in order to illustrate how the obtained results can be applied and interpreted for this special case. For general systems subjected to linear TDF, we derive the conditions on which the stability of a given system state changes, and characterize the properties of the corresponding bifurcation. The results hold both for ordinary and partial differential equations with TDF.

This thesis is organized as follows: Chapter 2 provides an introduction to the Swift–Hohenberg equation. Chapter 3 addresses stability properties of general systems subjected to time delayed feedback control and aims to characterize the linear time delayed feedback control mechanism from the theoretical point of view. Chapter 4 illustrates how these results apply to the Swift–Hohenberg equation with TDF and investigates the arising TDF–induced patterns. To conclude, we summarize the obtained results and outline open problems for future investigations in chapter 5.

2 The Swift-Hohenberg Equation

2.1 Introduction

In this chapter, we consider the Swift–Hohenberg equation and characterize its solutions and properties. To account for different phenomena, various modifications and variants of the classical Swift-Hohenberg equation have been proposed and studied. Here, we consider a generalized Swift-Hohenberg equation with an additional quadratic nonlinearity and analyze it as a model equation. The basic argumentation of this chapter will follow standard literature, such as [Bes06] and [CH93].

2.2 Structure and Properties

Let $\psi(\boldsymbol{r}, t)$ denote the order parameter of interest in a 2D spatially extended system, depending on space $\boldsymbol{r} = (x, y)$ and time $t \in \mathbb{R}_+$.

Consider a system which is described by the Swift-Hohenberg equation

$$\partial_t \psi(\boldsymbol{r}, t) = \left[\epsilon - (k_c^2 + \Delta)^2\right] \psi(\boldsymbol{r}, t) + \delta \cdot \psi(\boldsymbol{r}, t)^2 - \psi(\boldsymbol{r}, t)^3, \tag{2.1}$$

with the most unstable wave number[1] k_c and Laplace operator $\Delta = \nabla^2 = \partial_x^2 + \partial_y^2$. Equation (2.1) contains two parameters ϵ and δ which specify the strength of the linear and quadratic contribution, respectively.
For $\delta \neq 0$, inversion symmetry $\psi \to -\psi$ is broken and system states ψ with the same sign as δ are favoured on average. In general, the arising asymmetric solutions are called bright ($\delta > 0$) or dark ($\delta < 0$) structures.

For a partial differential equation, suitable boundary conditions have to be specified, and within this work, we consider periodic boundary conditions with periodicity L_x and L_y. Therefore, the domain of definition of the space variable $\boldsymbol{r}$ is $\boldsymbol{r} \in [0, L_x] \times [0, L_y]$ and periodicity yields:

$$\psi(\boldsymbol{r} + L_x \boldsymbol{e_x}, t) = \psi(\boldsymbol{r}, t), \tag{2.2}$$

$$\psi(\boldsymbol{r} + L_y \boldsymbol{e_y}, t) = \psi(\boldsymbol{r}, t). \tag{2.3}$$

[1] Without loss of generality, the most unstable wave number k_c can be set to $k_c = 1$ by a rescaling of variables. Nevertheless, it is useful to symbolically keep it as a point of reference.

Tranlational Invariance
The Swift-Hohenberg equation (2.1) is invariant to translations $\boldsymbol{r} \to \boldsymbol{r} + \boldsymbol{R}$ with translation vector $\boldsymbol{R}$, since the gradient $\boldsymbol{\nabla}$, as well as powers $\boldsymbol{\nabla}^n$ of $\boldsymbol{\nabla}$, are invariant to translations. This can be shown by iterative application of the chain rule.

Rotational Invariance
A rotation of $\boldsymbol{r}$ by an angle φ corresponds to rotation of the coordinate system by the angle $-\varphi$, which is a change of basis. The Laplace operator Δ is invariant to rotations, since it is the trace of the Hessian matrix[2] and the trace is basis invariant. Therefore, the Swift-Hohenberg equation (2.1) is invariant to rotations $\boldsymbol{r} \to \underline{\underline{R}}\, \boldsymbol{r}$ with the rotation matrix $\underline{\underline{R}}$.

Gradient System and Implications
The Swift-Hohenberg equation (2.1) is a gradient system, i.e., its dynamics can be expressed as a functional derivative of a Lyapunov functional [Bes06]:

$$\begin{aligned}\partial_t \psi(\boldsymbol{r}, t) &= \left[\epsilon - (k_c^2 + \Delta)^2\right] \psi(\boldsymbol{r}, t) + \delta \cdot \psi(\boldsymbol{r}, t)^2 - \psi(\boldsymbol{r}, t)^3 \\ &= -\frac{\delta L\left[\psi\right]}{\delta \psi(\boldsymbol{r}, t)},\end{aligned} \tag{2.4}$$

with the Lyapunov functional $L[\psi]$:

$$L\left[\psi\right] = \int -\frac{\epsilon}{2}\psi(\boldsymbol{r}, t)^2 + \frac{1}{2}\left[(k_c^2 + \Delta)\psi(\boldsymbol{r}, t)\right]^2 - \frac{\delta}{3}\psi(\boldsymbol{r}, t)^3 + \frac{1}{4}\psi(\boldsymbol{r}, t)^4 d\boldsymbol{r}. \tag{2.5}$$

The existence of a Lyapunov functional for a non-equilibrium system, like the Swift-Hohenberg equation, imposes strong restrictions on the system dynamics:

- Analogous to the minimization of free energy in equilibrium thermodynamics, long term solutions settle down to steady state solutions, which are given by the minima of the Lyapunov functional.
- Furthermore, the system is restricted to monotonous dynamics and the eigenvalues of the eigenvalue problem, which determines the linear stability of a system state, are real-valued[3].
- The possibility of oscillations or periodic solutions is ruled out.

Since the long term behaviour is governed by the steady states, we proceed with the analysis of steady states and their stability.

[2] The Hessian matrix H of a multivariate function $f(\boldsymbol{x})$ is the generalized second derivative, defined as $H_{i,j} = \partial_{x_i}\partial_{x_j} f$.
[3] In a rigorous proof, one can show that for every gradient system, the linearized operator is self-adjoint and therefore has real eigenvalues.

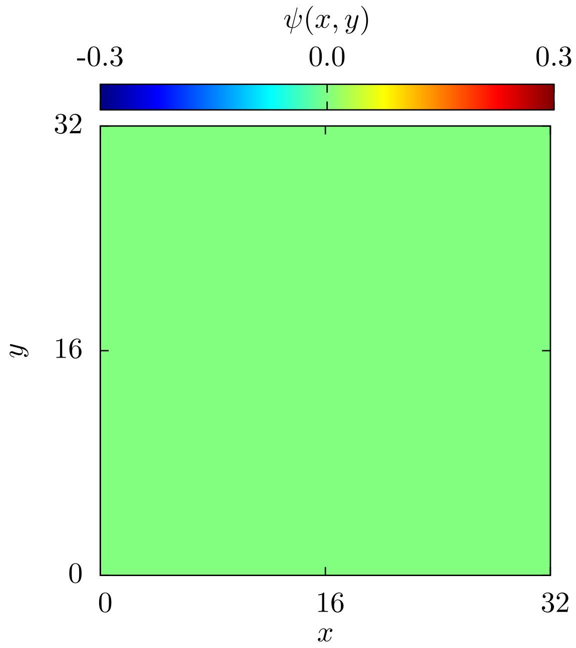

Figure 2.1: Homogeneous steady state $\psi(x, y) = 0$ obtained by numerical simulation of Eq. (2.1). Parameters are: $\epsilon = -1$, $\delta = 0$.

2.3 Steady State Solutions and Linear Stability

Steady state solutions of Eq. (2.1) are the **homogeneous steady state, stripes**[4] **and hexagons**, which can be found by numerical simulations.

Figure 2.1 shows a numerical simulation of the homogeneous steady state $\psi(\boldsymbol{r}) = 0$ and Fig. 2.2 shows non-trivial solutions with and without defects. Following [CH93], we denote patterns that contain only one orientation as *ideal patterns*, and denote patterns that consist of domains of ideal patterns with different orientations as *real patterns*. For real patterns, due to topology, there is a mismatch at the boundaries of the domains which creates defects. Real patterns are more likely, especially for large growth rates or large systems, when the growth of domains is faster than the interaction which aligns them. Before investigating real patterns, the ideal patterns of which they consist have to be understood.

Therefore, within this thesis, we focus on ideal patterns and their linear stability.

[4] Stripes are the 2D analogue of 3D rolls. One obtains stripes by considering a cross-section of rolls.

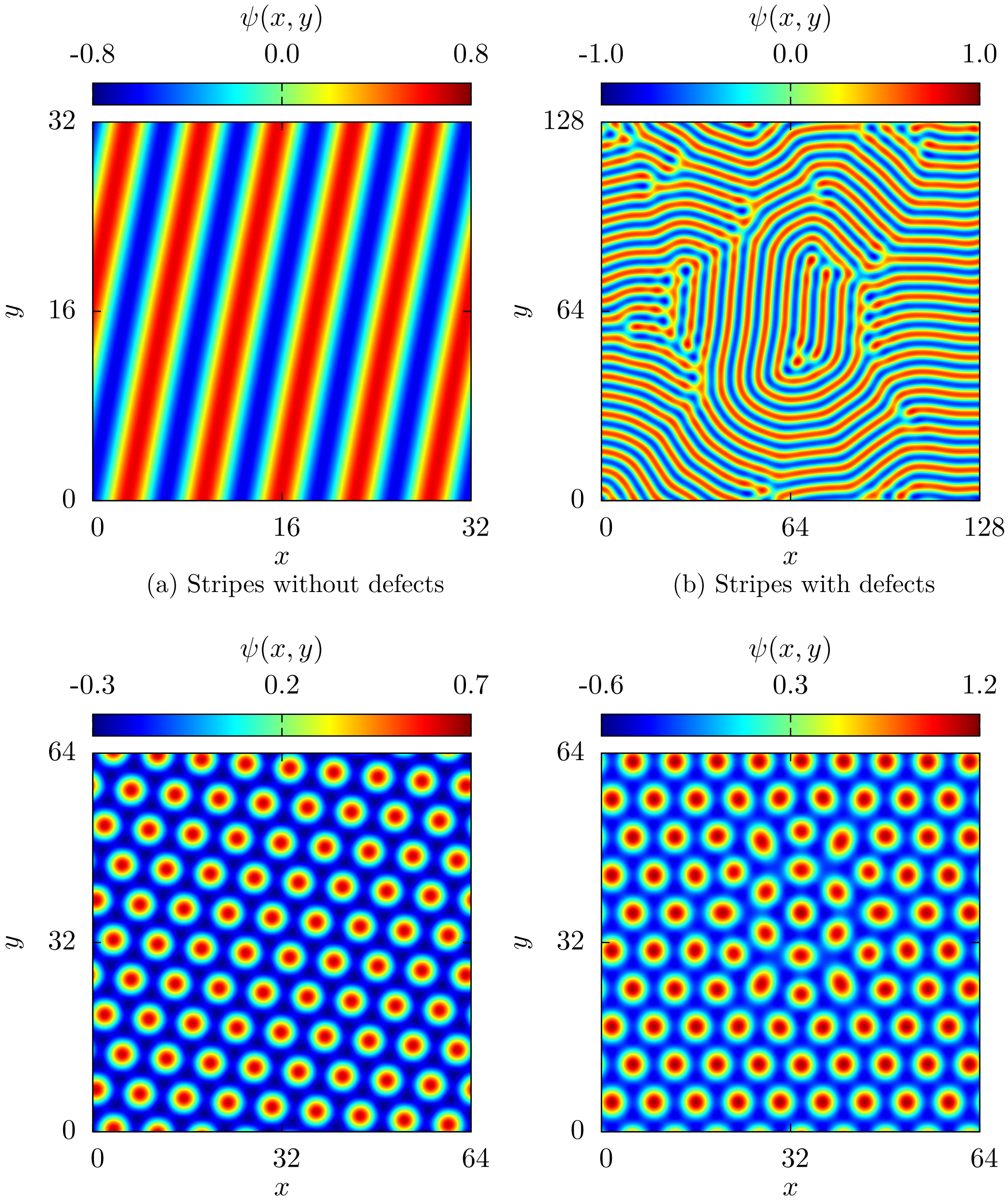

(a) Stripes without defects

(b) Stripes with defects

(c) Hexagons without defects

(d) Hexagons with defects

Figure 2.2: Snapshots of non–trivial solutions of the Swift-Hohenberg equation (2.1) with and without defects. Parameters are: a), b): $\epsilon = 0.3$, $\delta = 0$ c): $\epsilon = 0.05$, $\delta = 0.5$, d): $\epsilon = 0.05$, $\delta = 1$. Initial conditions: $\psi(\boldsymbol{r}, 0) = 0$+noise.

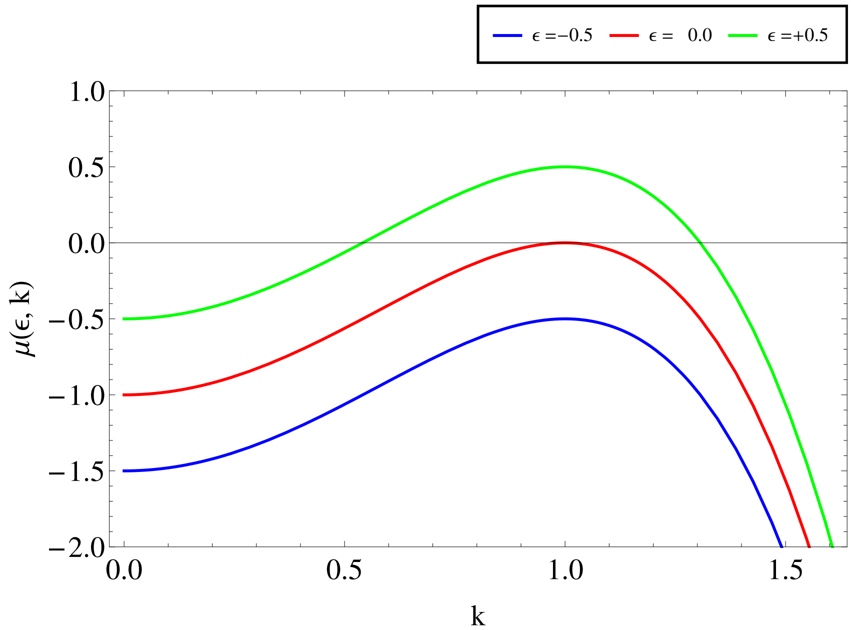

Figure 2.3: Growth rate μ vs. wave number k for different values of ϵ. The plane wave perturbation grows if $\mu > 0$ and decays otherwise.

2.3.1 Homogeneous Steady State

The homogeneous steady state is given by $\psi^{(0)}(\boldsymbol{r}) = 0$. To analyze its linear stability, we substitute

$$\psi(\boldsymbol{r}, t) = \psi^{(0)} + \eta(\boldsymbol{r}, t) \tag{2.6}$$

in the Swift-Hohenberg equation (2.1) and derive the linearized equation for the small perturbation η:

$$\partial_t \eta(\boldsymbol{r}, t) = \left[\epsilon - (k_c^2 + \Delta)^2\right] \eta(\boldsymbol{r}, t). \tag{2.7}$$

To solve the above equation, we consider plane wave perturbations $\eta(\boldsymbol{r}, t)$ with wave vector $\boldsymbol{k}$ and growth rate μ

$$\eta(\boldsymbol{r}, t) = e^{\mu t} e^{i\boldsymbol{k}\boldsymbol{r}} + c.c., \tag{2.8}$$

where $c.c.$ denotes the complex conjugate of the preceding term. The resulting growth rate $\mu(\epsilon, k)$

$$\mu(\epsilon, k) = \epsilon - (k_c^2 - k^2)^2 \tag{2.9}$$

is shown in Fig. 2.3 for different values of ϵ. Figure 2.3 illustrates that the homoge-

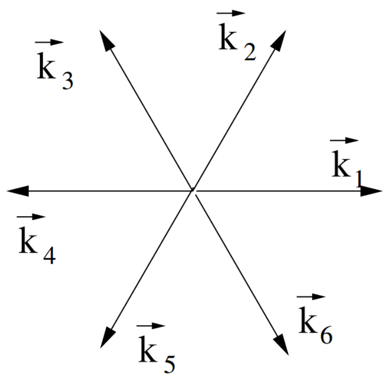

Figure 2.4: Representation of hexagons and stripes as a superposition of plane waves with wave vectors $\vec{k}_j$, $j = 1, .., 6$. Two plane waves with opposite wave vectors yield stripes and a superposition of three stripe patterns yields hexagons. The six wave vectors have length $|\vec{k}| = k_c$. Figure taken from [Bes06].

neous steady state is linearly stable if

$$\epsilon \leq 0 \tag{2.10}$$

and unstable if

$$\epsilon > 0. \tag{2.11}$$

Therefore, the paramater ϵ can be considered as the distance from the bifurcation point, where linear stability of the homogeneous steady state changes.

2.3.2 Competition between Stripes and Hexagons - a General Ansatz

Numerical simulations reveal that stripes and hexagons arise for different values of ϵ and δ and therefore we analyze under which conditions they exist and under which conditions they are stable. To investigate the competition between stripes and hexagons, we make a general ansatz which incorporates both patterns as a special case. Then, we derive amplitude equations [Seg69] which allow us to conclude existence and stability properties for the particular pattern. To this end, a superposition of stripes with wave vectors $\boldsymbol{k}_j$ is considered, in which the wave vectors $\boldsymbol{k}_j$ are arranged in a hexagonal form. The basic idea is illustrated in Fig. 2.4.

Since the wave vectors pairwise only differ in sign, it is sufficient to consider either the wave vectors with odd or even indices in Fig. 2.4. Taking the wave vectors[5] $\vec{k}_j$ with odd indices and renaming them as $\boldsymbol{k}_j$, $j = 1, 2, 3$, one obtains the ansatz

$$\psi(\boldsymbol{r}, t) = \sum_{j=1}^{3} \xi_j e^{i\boldsymbol{k_j r}} + c.c. \tag{2.12}$$

$$= \sum_{j=1}^{3} |\xi_j| \cos(\boldsymbol{k}_j \boldsymbol{r} + \varphi_j), \tag{2.13}$$

with amplitudes $\xi_j(t) \in \mathbb{C}$ and wave vectors $\boldsymbol{k}_j$:

$$\boldsymbol{k}_1 = k_c \begin{pmatrix} 1 \\ 0 \end{pmatrix}, \quad \boldsymbol{k}_2 = \frac{k_c}{2} \begin{pmatrix} -1 \\ \sqrt{3} \end{pmatrix}, \quad \boldsymbol{k}_3 = \frac{k_c}{2} \begin{pmatrix} -1 \\ -\sqrt{3} \end{pmatrix}. \tag{2.14}$$

The amplitudes $\xi_j(t) \in \mathbb{C}$ can be complex and their phases φ_j shift the corresponding pattern along the direction of their wave vectors $\boldsymbol{k}_j$. This ansatz contains both stripes and hexagons. When considering

$$|\xi_1| = |\xi_2| = |\xi_3| \tag{2.15}$$

one obtains hexagons, whereas

$$|\xi_1| \neq 0, \quad |\xi_2| = |\xi_3| = 0. \tag{2.16}$$

yields stripes. The non–zero amplitude $|\xi_j| \neq 0$ can be arbitrarily chosen.

To investigate the competition between stripes and hexagons, a criterion can be derived which specifies under which conditions the system state converges to the stripe solution (2.16) or to the hexagon solution (2.15). To this end, we derive *amplitude equations*, i.e., evolution equations for the complex amplitudes $\xi_j(t) \in \mathbb{C}$, without assuming stripes or hexagons yet. This can be done by a *mode projection technique*. The basic idea is to make an ansatz for the relevant modes[6] and focus on the system dynamics in the subspace which is spanned by the modes of the ansatz. Technically, the system dynamics is projected on the subspace and the dynamical behaviour in the subspace is analyzed. In the present case the mode projection technique works as follows:

1. The ansatz for stripes and hexagons (2.12) is substituted in the Swift-Hohenberg equation (2.1).

[5] Two different notations are used, in order to formally distinguish between all possible wave vectors which build the hexagon, denoted as $\vec{k}_j$, and the relevant, non-redundant wave vectors $\boldsymbol{k}_j$.

[6] By definition, the relevant modes govern the system dynamics. The utility of the method crucially depends on the ansatz and the identification of these modes.

2. Thereby, the nonlinear terms in the Swift-Hohenberg equation (2.1) generate interactions between different plane waves and also lead to higher order contributions.

3. The resulting equation is projected on the subspace, which is spanned by the plane waves $e^{i\boldsymbol{k}_j\boldsymbol{r}}$. This results in evolution equations for their amplitudes $\xi_j(t)$.

The projection of a term A can be either carried out by evaluating $\langle e^{i\boldsymbol{k}_j\boldsymbol{r}}|A\rangle\, e^{i\boldsymbol{k}_j\boldsymbol{r}}$, with the L^2 scalar product $\langle\cdot|\cdot\rangle$, or by collecting terms of order $\mathcal{O}(e^{i\boldsymbol{k}_j\boldsymbol{r}})$ within A. The resulting amplitude equations read [Bes06]:

$$\dot{\xi}_1 = \epsilon\xi_1 + 2\delta\xi_2^*\xi_3^* - 3\xi_1\left[|\xi_1|^2 + 2|\xi_2|^2 + 2|\xi_3|^2\right], \tag{2.17a}$$

$$\dot{\xi}_2 = \epsilon\xi_2 + 2\delta\xi_3^*\xi_1^* - 3\xi_2\left[2|\xi_1|^2 + |\xi_2|^2 + 2|\xi_3|^2\right], \tag{2.17b}$$

$$\dot{\xi}_3 = \epsilon\xi_3 + 2\delta\xi_1^*\xi_2^* - 3\xi_3\left[2|\xi_1|^2 + 2|\xi_2|^2 + |\xi_3|^2\right]. \tag{2.17c}$$

For further analysis of the amplitude equations (2.17), it is convenient to represent the complex amplitude $\xi_j(t) \in \mathbb{C}$ as $\xi_j(t) = R_j(t)e^{i\varphi_j(t)}$ and split the amplitude equations (2.17) into the real amplitude $R_j(t)$ and phase $\varphi_j(t)$, which yields:

$$\dot{R}_1 = \epsilon R_1 + 2\delta \cdot R_2R_3\cos(\varphi_1+\varphi_2+\varphi_3) - 3R_1\left[R_1^2 + 2R_2^2 + 2R_3^2\right], \tag{2.18a}$$
$$\dot{R}_2 = \epsilon R_2 + 2\delta \cdot R_3R_1\cos(\varphi_1+\varphi_2+\varphi_3) - 3R_2\left[2R_1^2 + R_2^2 + 2R_3^2\right], \tag{2.18b}$$
$$\dot{R}_3 = \epsilon R_3 + 2\delta \cdot R_1R_2\cos(\varphi_1+\varphi_2+\varphi_3) - 3R_3\left[2R_1^2 + 2R_2^2 + R_3^2\right], \tag{2.18c}$$
$$R_1\dot{\varphi}_1 = -2\delta \cdot R_2R_3\sin(\varphi_1+\varphi_2+\varphi_3), \tag{2.18d}$$
$$R_2\dot{\varphi}_2 = -2\delta \cdot R_3R_1\sin(\varphi_1+\varphi_2+\varphi_3), \tag{2.18e}$$
$$R_3\dot{\varphi}_3 = -2\delta \cdot R_1R_2\sin(\varphi_1+\varphi_2+\varphi_3). \tag{2.18f}$$

Equation (2.18) can be written in vector form

$$\begin{pmatrix} \dot{R}_1 \\ \dot{R}_2 \\ \dot{R}_3 \\ R_1\dot{\varphi}_1 \\ R_2\dot{\varphi}_2 \\ R_3\dot{\varphi}_3 \end{pmatrix} = \boldsymbol{F}[R_1, R_2, R_3, \varphi_1, \varphi_2, \varphi_3], \tag{2.19}$$

$$\underset{\text{represent as}}{\Longleftrightarrow} \quad \dot{\boldsymbol{x}} = \boldsymbol{F}[\boldsymbol{x}], \tag{2.20}$$

with the multivariate vector-valued function $\boldsymbol{F}[R_1, R_2, R_3, \varphi_1, \varphi_2, \varphi_3]$ defined as the right hand side of Eq. (2.18).

Let $R_j^{(0)}$, $\varphi_j^{(0)}$, $j = 1, 2, 3$ be the stripe or the hexagon steady state solution of Eq. (2.18). To analyze their stability, we consider

$$R_j(t) = R_j^{(0)} + \delta R_j(t), \tag{2.21}$$

$$\varphi_j(t) = \varphi_j^{(0)} + \delta\varphi_j(t), \tag{2.22}$$

with small perturbations of amplitude $\delta R_j(t)$ and phase $\delta\varphi_j(t)$. The evolution of the small perturbations is determined by the linearization $\underline{\underline{F'}}$ of $\boldsymbol{F}$, being evaluated at the steady state. Representing the steady state by $\boldsymbol{x}^{(0)}$ and perturbations by $\boldsymbol{\delta x}$, the linear stability problem can be written as

$$\dot{\boldsymbol{\delta x}} = \underline{\underline{F'}} \cdot \delta\boldsymbol{x}. \tag{2.23}$$

The linearization $\underline{\underline{F'}}$ of $\boldsymbol{F}[\boldsymbol{x}]$ is given by the Jacobian matrix evaluated at the steady state

$$\underline{\underline{F'}} = \left(\frac{\partial F_i}{\partial x_j}\right)_{i,j}, \tag{2.24}$$

where F_i and x_j are the i^{th} and j^{th} component of $\boldsymbol{F}$ and $\boldsymbol{x}$, respectively. In the context of linear stability analysis, the Jacobian matrix evaluated at the steady state $\boldsymbol{x}^{(0)}$ is also referred to as the stability matrix $\underline{\underline{S}}$.
The general solution $\boldsymbol{\delta x}$ of Eq. (2.23) is given in terms of eigenvectors $\boldsymbol{v}_j$ and eigenvalues μ_j of $\underline{\underline{S}}$

$$\boldsymbol{\delta x}(t) = \sum_j C_j \, e^{\mu_j t} \, \boldsymbol{v}_j, \tag{2.25}$$

with constant amplitudes C_j. The steady state solution $\boldsymbol{x}^{(0)}$ is linearly stable if $\boldsymbol{\delta x} \to 0$ and unstable otherwise. In terms of eigenvalues μ_j, the steady state solution $\boldsymbol{x}^{(0)}$ is stable if all $\mu_j \leq 0$ and unstable if any $\mu_j > 0$.

To investigate the competition between stripes and hexagons, we analyze under which conditions they are stable, i.e., under which conditions the corresponding linear stability problem has negative eigenvalues $\mu_j \leq 0$.

2.3.3 Stripes

The stripes steady state solution is determined by Eq. (2.16) and by the steady state condition ($\dot{\xi}_j = 0 \leftrightarrow \dot{R}_j = 0,\ \dot{\varphi}_j = 0$) for Eq. (2.18). It is given by:

$$R_1^{(0)} = \sqrt{\frac{\epsilon}{3}}, \quad R_2^{(0)} = R_3^{(0)} = 0, \tag{2.26a}$$

$$\varphi_1^{(0)} : \text{random}, \quad \varphi_2^{(0)}, \varphi_3^{(0)} : \text{indeterminate}. \tag{2.26b}$$

Since the amplitude $R_1^{(0)}$ must be real-valued, stripes only exist for

$$\epsilon \geq 0. \tag{2.27}$$

The random phase φ_1 reflects the translational invariance. As the shifted solution has the same stability properties as the unshifted solution, we consider the solution with

$$\varphi_1 = 0, \tag{2.28}$$

and analyze the corresponding linear stability problem.

Amplitude Perturbations

For the small perturbations $\delta R_j(t)$ of the real amplitude $R_j^{(0)}$, one obtains:

$$\frac{d}{dt}\begin{pmatrix}\delta R_1(t)\\ \delta R_2(t)\\ \delta R_3(t)\end{pmatrix} = \underbrace{\begin{pmatrix}-2\epsilon & 0 & 0\\ 0 & -\epsilon & 2\delta \cdot R_1^{(0)}\\ 0 & 2\delta \cdot R_1^{(0)} & -\epsilon\end{pmatrix}}_{=:\underline{\underline{S}}^R} \cdot \begin{pmatrix}\delta R_1(t)\\ \delta R_2(t)\\ \delta R_3(t)\end{pmatrix}. \tag{2.29}$$

The eigenvalues μ_j^R and eigenvectors $\boldsymbol{v}_j^R$ of the stability matrix $\underline{\underline{S}}^R$ are:

$$\mu_1^R = -2\epsilon, \qquad \boldsymbol{v}_1^R = \begin{pmatrix}1\\0\\0\end{pmatrix}, \tag{2.30}$$

$$\mu_2^R = -\epsilon - 2\delta \cdot R_1^{(0)}, \quad \boldsymbol{v}_2^R = \begin{pmatrix}0\\-1\\1\end{pmatrix}, \tag{2.31}$$

$$\mu_3^R = -\epsilon + 2\delta \cdot R_1^{(0)}, \quad \boldsymbol{v}_3^R = \begin{pmatrix}0\\1\\1\end{pmatrix}. \tag{2.32}$$

Before analyzing the stability properties, we want to give an intuitive interpretation of the eigenvectors $\boldsymbol{v}_j^R$. Consider a setting in which the stripes solution is stable and parameters are changed such that one of the eigenvalues μ_j^R becomes positive. Then, the coefficients of the corresponding eigenvector $\boldsymbol{v}_j^R$ specify which perturbations δR_j grow and towards which solution the system state is driven.

- If $\mu_1^R > 0$, then perturbations δR_1 to the amplitude $R_1^{(0)}$ start to grow.
- If $\mu_2^R > 0$ or $\mu_3^R > 0$, then perturbations δR_2 and δR_3 start to grow.

A closer inspection of the eigenvectors $\boldsymbol{v}_j^R$ and eigenvalues μ_j^R therefore suggests that for

$$\mu_1^R > 0 \mid \mu_2^R > 0 \mid \mu_3^R > 0$$

the system is driven towards the following states, respectively:

homogeneous | dark hexagons | bright hexagons

Further analysis will show that this is the case and will give additional information about the resulting states.

To analyze the stability of stripes, we consider on which condition all eigenvalues μ_j^R are negative. This yields:

$$\mu_1^R \leq 0 \Leftrightarrow \epsilon \geq 0, \tag{2.33}$$

$$\mu_2^R, \mu_3^R \leq 0 \Leftrightarrow \epsilon \geq \frac{4}{3}\delta^2. \tag{2.34}$$

To sum up, stripes are stable, if

$$\epsilon \geq \frac{4}{3}\delta^2. \tag{2.35}$$

Phase Perturbations

For a small perturbation $\delta\varphi_1(t)$ of phase $\varphi_1^{(0)}$ one obtains:

$$\frac{d}{dt}\ \delta\varphi_1(t) = 0 \cdot \delta\varphi_1(t) = 0. \tag{2.36}$$

The eigenvalue μ^φ of the phase problem is

$$\mu^\varphi = 0, \tag{2.37}$$

which denotes neutral stability with respect to phase perturbations, as a result of translational invariance.

2.3.4 Hexagons

The hexagon steady state solution is determined by Eq. (2.15) and by the steady state condition ($\dot{\xi}_j = 0 \leftrightarrow \dot{R}_j = 0,\ \dot{\varphi}_j = 0$) for Eq. (2.18). It reads:

$$R_1^{(0)} = R_2^{(0)} = R_3^{(0)} \overset{\text{def.}}{=} R_h = \frac{1}{15}\left((-1)^n \delta \pm \sqrt{\delta^2 + 15\epsilon}\right), \tag{2.38a}$$

$$\varphi_1^{(0)} + \varphi_2^{(0)} + \varphi_3^{(0)} = n\pi, \quad n \in \mathbb{Z}. \tag{2.38b}$$

Since the hexagon steady state amplitude R_h is real-valued, hexagons only exist for

$$\epsilon \geq -\frac{1}{15}\delta^2. \tag{2.39}$$

We want to emphasize a detail which typically is not relevant, but in this case creates a paradox, the resolution of which contains valuable information about the structure of hexagons.

It can be seen that for certain n, δ and ϵ, the amplitude $R_j^{(0)}$ of the steady state hexagon solution can be negative. It seems counterintuitive, since the amplitude of a complex number is also referred to as its absolute value, which by definition is positive. To resolve this problem, consider the following two representations of a complex number ξ:

$$\xi = Re^{i\varphi} = Re^{i\varphi} \cdot (-1) \cdot (-1) = \underbrace{-R}_{=:\widetilde{R}} e^{i(\varphi+\pi)}.$$

The same complex number ξ can be represented by amplitude $R \geq 0$ and phase φ, but also with negative amplitude $\widetilde{R} \leq 0$ and phase $\varphi + \pi$. Though both representations yield the same result, it is convention to use the first representation and fully encode orientation within the phase φ.

We see that for the hexagon steady state solution both representations naturally arise at the same time and from the point of view of convention, negative $R_j^{(0)}$ correspond to a phase shift $\varphi^{(0)} \to \varphi^{(0)} + \pi$. This view is self-consistent, as thereby n changes from odd to even or vice versa and thereby ensures that $R_j^{(0)}$ remains positive.

The $\pm$ sign in $R_j^{(0)}$ reflects that there is a large amplitude solution and a small amplitude solution which both build a hexagonal lattice.
The large amplitude solution corresponds to the spots[7] which build the hexagonal lattice. Bright spots arise for $\delta > 0$ and dark spots for $\delta < 0$. Therefore, the pattern they build is termed as *bright or dark hexagons*. The small amplitude solution

[7] The spots can either have large positive or large negative amplitude and are called bright or dark spots, respectively.

represents the gaps in between these spots, which also build a hexagonal lattice. The occurrence of the spots and gaps both building a hexagonal lattice was already observed in the numerical simulation in Fig. 2.2c, which shows bright hexagons.

In the hexagon steady state solution, two of three phases are random and the third phase is determined by the steady state condition. The two independent phases can be set to arbitrary values, which reflects translation symmetry in the 2D system. As the shifted solution has the same properties as the unshifted solution, we consider the solution with

$$\varphi_1 = 0, \quad \varphi_2 = 0, \tag{2.40}$$

$$\Rightarrow \varphi_3 = 0. \tag{2.41}$$

To analyze the stability of hexagons, we consider the corresponding linear stability problem.

Amplitude Perturbations

For the small perturbations $\delta R_j(t)$ of the amplitudes $R_j^{(0)}$, one obtains

$$\frac{d}{dt}\begin{pmatrix}\delta R_1(t)\\ \delta R_2(t)\\ \delta R_3(t)\end{pmatrix} = \underbrace{\begin{pmatrix}A & B & B\\ B & A & B\\ B & B & A\end{pmatrix}}_{=:\underline{\underline{S}}^R} \cdot \begin{pmatrix}\delta R_1(t)\\ \delta R_2(t)\\ \delta R_3(t)\end{pmatrix}, \tag{2.42}$$

where $A = \epsilon - 21R_h^2$ and $B = 2\delta \cdot R_h - 12R_h^2$. The eigenvalues μ_j^R and eigenvectors $\boldsymbol{v}_j^R$ of the stability matrix $\underline{\underline{S}}^R$ are:

$$\mu_1^R = A - B, \quad \boldsymbol{v}_1^R = \begin{pmatrix}-1\\ 0\\ 1\end{pmatrix}, \tag{2.43}$$

$$\mu_2^R = A - B, \quad \boldsymbol{v}_2^R = \begin{pmatrix}-1\\ 1\\ 0\end{pmatrix}, \tag{2.44}$$

$$\mu_3^R = A + 2B, \quad \boldsymbol{v}_3^R = \begin{pmatrix}1\\ 1\\ 1\end{pmatrix}. \tag{2.45}$$

The eigenvectors $\boldsymbol{v}_j^R$ determine how hexagons can become unstable and towards which solution the system state is driven according to linear stability analysis:

- If $\mu_1^R = \mu_2^R > 0$, the system is driven towards the stripe solution.
- If $\mu_3^R > 0$, the system is driven towards the homogeneous solution.

To analyze the stability of hexagons with respect to perturbations to their amplitude, we consider under which conditions all eigenvalues are negative. This yields:

$$\mu_1^R = \mu_2^R \leq 0 \Leftrightarrow \epsilon \leq \frac{16}{3}\delta^2, \tag{2.46}$$

$$\mu_3^R \leq 0 \Leftrightarrow \epsilon \geq -\frac{1}{15}\delta^2. \tag{2.47}$$

To sum up, hexagons are stable with respect to perturbations δR_j if

$$-\frac{1}{15}\delta^2 \leq \epsilon \leq \frac{16}{3}\delta^2. \tag{2.48}$$

Notice that on the bifurcation curve $\epsilon = -\frac{1}{15}\delta^2 < 0$, hexagons arise in a subcritical bifurcation with finite amplitude $R_h = \delta$ and are supercritical for $\epsilon > 0$ [Bes06].

Phase Perturbations

For the small perturbations $\delta\varphi_j(t)$ of the phases $\varphi_j^{(0)}$, one obtains the following linear stability problem:

$$\frac{d}{dt}\begin{pmatrix}\delta\varphi_1(t)\\ \delta\varphi_2(t)\\ \delta\varphi_3(t)\end{pmatrix} = \underbrace{-2\delta \cdot R_h \begin{pmatrix}1 & 1 & 1\\ 1 & 1 & 1\\ 1 & 1 & 1\end{pmatrix}}_{=:\underline{\underline{S}}^\varphi} \cdot \begin{pmatrix}\delta\varphi_1(t)\\ \delta\varphi_2(t)\\ \delta\varphi_3(t)\end{pmatrix}. \tag{2.49}$$

The eigenvalues μ_j^φ and eigenvectors $\boldsymbol{v}_j^\varphi$ of the stability matrix $\underline{\underline{S}}^\varphi$ are:

$$\mu_1^\varphi = 0, \qquad \boldsymbol{v}_1^\varphi = \begin{pmatrix}-1\\ 0\\ 1\end{pmatrix}, \tag{2.50}$$

$$\mu_2^\varphi = 0, \qquad \boldsymbol{v}_2^\varphi = \begin{pmatrix}-1\\ 1\\ 0\end{pmatrix}, \tag{2.51}$$

$$\mu_3^\varphi = -6\delta R_h, \quad \boldsymbol{v}_3^\varphi = \begin{pmatrix}1\\ 1\\ 1\end{pmatrix}. \tag{2.52}$$

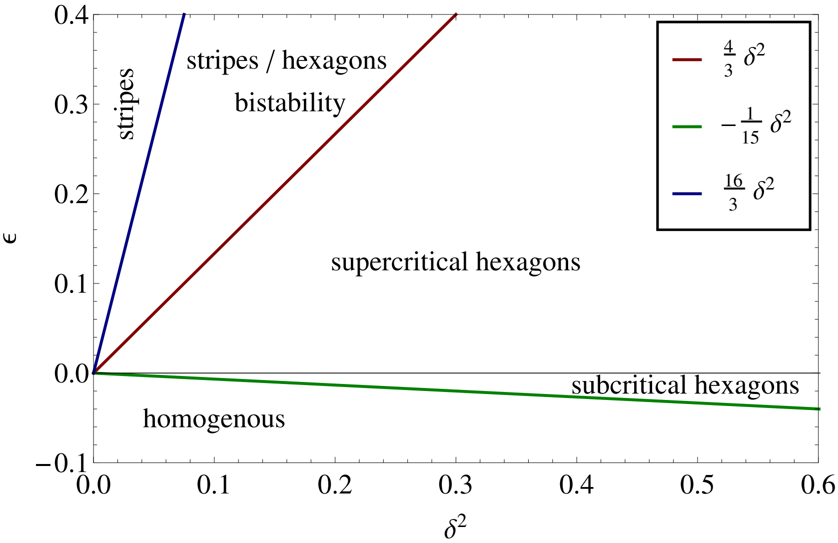

Figure 2.5: Stability regions of the homogeneous steady state, stripes and hexagons on the (δ^2, ϵ) plane. For given ϵ and δ the corresponding region specifies which solutions are stable. The stability boundaries are obtained by linear stability analysis.

The eigenvectors $\boldsymbol{v}_1^\varphi$ and $\boldsymbol{v}_2^\varphi$ indicate tranlations in space and the eigenvector $\boldsymbol{v}_3^\varphi$ is a non-trivial representation of a zero-translation and represents a closed loop. This artefact arises since we have chosen three wavevectors $\boldsymbol{k}_j, j = 1, 2, 3$ to represent 2D hexagons and therefore only two out of three $\boldsymbol{k}_j$ are linearly independent and $\boldsymbol{k}_1 + \boldsymbol{k}_2 + \boldsymbol{k}_3 = 0$ represents a closed loop.

To conclude, the steady state hexagons are neutrally stable with respect to translations as expected from translational symmetry.

2.4 Results of Linear Stability Analysis

We want to summarize the results obtained for the linear stability of steady state solutions of the Swift-Hohenberg equation (2.1). The steady state solutions are neutrally stable with respect to translations and their stability with respect to amplitude perturbations depends on the parameters ϵ and δ. Analogous to [Bes06], Fig. 2.5 shows bifurcation curves and stability regions of the homogeneous steady state, stripes and hexagons vs. system parameters ϵ and δ. Note that although a bistable region of stripes and hexagons is predicted according to linear stability analysis, for long times only the state which minimizes the Lyapunov functional L

persists.

2.5 Direct Numerical Simulation

For a direct numerical simulation of the Swift-Hohenberg equation (2.1), we use a *pseudo-spectral method* [Boy13] in space and a *semi–implicit Euler* scheme [SK09] for time stepping.

To this end, we split the Swift-Hohenberg equation into the contributions which are linear in ψ and which are nonlinear in ψ and denote them as $L(\Delta)\psi$ and $N[\psi]$, respectively. In real space one obtains:

$$\begin{aligned}\partial_t\psi(\boldsymbol{r},t) &= \underbrace{\left[\epsilon-(k_c^2+\Delta)^2\right]}\psi(\boldsymbol{r},t)+\underbrace{\delta\psi(\boldsymbol{r},t)^2-\psi(\boldsymbol{r},t)^3}\\ &= \qquad L(\Delta)\qquad\psi(\boldsymbol{r},t)+\qquad N[\psi].\end{aligned} \tag{2.53}$$

In Fourier space, this yields:

$$\partial_t\widetilde{\psi}(\boldsymbol{k},t) = \quad L(-k^2)\quad\widetilde{\psi}(\boldsymbol{k},t)+\quad\widetilde{N}(\boldsymbol{k},t), \tag{2.54}$$

where $\widetilde{N}=\mathrm{FT}[N]$ is the Fourier transform of N.

The basic idea of the pseudo-spectral method is the observation that it is advantageous to treat the linear contribution $L(-k^2)\widetilde{\psi}$ in Fourier space and to treat the nonlinear contribution $N[\psi]$ in real space and therefore to switch between both spaces as necessary. The advantages are:

- In Fourier space the linear part $L(-k^2)\widetilde{\psi}$ is local and its computation can be caried out by a multiplication instead of an application of a differential operator.
- In real space the nonlinearity $N[\psi]$ is local and can be carried out by a multiplication, whereas in Fourier space it would involve convolutions whose computation is time consuming.
- Making use of the Fast Fourier Transformation allows to switch between spaces very efficiently in $\mathcal{O}(n\log(n))$ operations instead of $\mathcal{O}(n^2)$.

The pseudo–spectral method can be combined with the semi–implicit Euler time stepping as follows: Let dt denote the time step in the time discretization and consider the spatial Fourier transform $\widetilde{\psi}(\boldsymbol{k},t)$ of a field $\psi(\boldsymbol{r},t)$. Then, the semi–implicit Euler time stepping in Fourier space reads

$$\frac{\widetilde{\psi}(\boldsymbol{k},t+dt)-\widetilde{\psi}(\boldsymbol{k},t)}{dt} = L(-k^2)\widetilde{\psi}(\boldsymbol{k},t+dt)+\widetilde{N}(\boldsymbol{k},t), \tag{2.55}$$

$$
\begin{array}{ccc}
\psi(\boldsymbol{r},t) & \longrightarrow & N[\psi(\boldsymbol{r},t)] \\
\Big\downarrow \text{FT} & & \Big\downarrow \text{FT} \\
\widetilde{\psi}(\boldsymbol{k},t) & & \widetilde{N}(\boldsymbol{k},t) \\
\Big\downarrow & & \Big\downarrow
\end{array}
$$

$$
\boxed{\widetilde{\psi}(\boldsymbol{k},t+dt) = \frac{1}{dt^{-1} - L(-k^2)} \left[\frac{\widetilde{\psi}(\boldsymbol{k},t)}{dt} + \widetilde{N}(\boldsymbol{k},t) \right]}
$$

$$
\Big\downarrow \text{FT}^{-1}
$$

$$
\psi(\boldsymbol{r},t+dt)
$$

Figure 2.6: Data flow of the numerical treatment. We use a pseudo-spectral method in space and a semi–implicit Euler time stepping for time integration.

which explicitly yields the next time step $\widetilde{\psi}(\boldsymbol{k},t+dt)$:

$$
\widetilde{\psi}(\boldsymbol{k},t+dt) = \frac{\widetilde{\psi}(\boldsymbol{k},t) + dt \cdot \widetilde{N}(\boldsymbol{k},t)}{1 - dt \cdot L(-k^2)} \tag{2.56}
$$

Switching from Fourier space back to real space then yields the next time step $\psi(\boldsymbol{r},t+dt)$. The semi–implicit Euler scheme inherits the unconditional numerical stability which is typical for implicit numerical schemes, but still yields an explicit form of the new time step as is typical for explicit schemes. Figure 2.6 illustrates the data flow of our numerical treatment.

All simulations are done with the following discretization for space $\boldsymbol{r} = (x,y)$ and time t:

$$
dx = 0.1, \;\; dy = 0.1, \;\; dt = 0.1
$$

3 General Systems with Time Delayed Feedback Control

3.1 Motivation and Introduction

In this chapter, we investigate the influence of the linear time delayed feedback control mechanism on the stability properties of general systems.

Let $\boldsymbol{\psi}(\boldsymbol{r},t)$ denote a system state which depends on space $\boldsymbol{r} \in \mathbb{R}^n$ and time t in a spatially extended system. We consider the case in which the re–injected signal $\boldsymbol{s}(\boldsymbol{\psi})$ is equal to the system variable $\boldsymbol{\psi}$, i.e., $\boldsymbol{s}(\boldsymbol{\psi})$ is given by the identity function $\boldsymbol{s}(\boldsymbol{\psi}) = \boldsymbol{\psi}$. Then, the corresponding feedback signal $\boldsymbol{s}(\boldsymbol{\psi})$ is linear and we denote the mechanism as *linear time delayed feedback control.* Equation (1.1) then becomes

$$\partial_t \boldsymbol{\psi}(\boldsymbol{r},t) = \boldsymbol{F}[\boldsymbol{\psi}] + \underline{\underline{K}}\ (\boldsymbol{\psi}(\boldsymbol{r},t) - \boldsymbol{\psi}(\boldsymbol{r},t-\tau)), \tag{3.1}$$

where the non–linear operator $\boldsymbol{F}[\boldsymbol{\psi}]$ represents the intrinsic system dynamics. We denote the special case where $\underline{\underline{K}}$ is a scalar matrix $\underline{\underline{K}} = \alpha \cdot \underline{\underline{1}}$ as *scalar coupling* or *scalar TDF* and denote the general case as *non–scalar coupling* or *non–scalar TDF*. The factor α in the scalar TDF describes the strength of the delayed feedback and therefore is denoted as *delay strength* α. For scalar coupling, Eq. (3.1) results in:

$$\partial_t \boldsymbol{\psi}(\boldsymbol{r},t) = \boldsymbol{F}[\boldsymbol{\psi}] + \alpha \cdot \underline{\underline{1}}\ (\boldsymbol{\psi}(\boldsymbol{r},t) - \boldsymbol{\psi}(\boldsymbol{r},t-\tau)). \tag{3.2}$$

In this chapter, we consider the limit of small delay times τ for scalar TDF, and perform a linear stability analysis for scalar and non–scalar coupling for a general system.
When performing a linear stability analysis for a general system state subjected to TDF, one can calculate under which conditions a given eigenmode $\boldsymbol{\varphi}_j$ changes stability and calculate the corresponding eigenvalue λ_j. However, the interpretation of $\boldsymbol{\varphi}_j$ changing stability can only be made in the context what the eigenmode $\boldsymbol{\varphi}_j$ represents in the particular system.

For the sake of concreteness, after deriving the general results, we apply our approach for the Swift–Hohenberg equation (2.1) with time delayed feedback. Note that for the special case of a one–component system, the system state $\boldsymbol{\psi}$ as well as the coupling matrix $\underline{\underline{K}}$ become scalars and the results for TDF with scalar coupling matrices can be applied.

3.2 Limit of Small Delay Times

Consider the time delayed feedback control term in equation (3.2) for small delay times τ. Let the delay time τ be small enough, such that the approximation by a Taylor expansion up to first order can be justified, and expand the control term at time t:

$$\begin{aligned}\boldsymbol{\psi}(\boldsymbol{r},t) - \boldsymbol{\psi}(\boldsymbol{r},t-\tau) &= \boldsymbol{\psi}(\boldsymbol{r},t) - \Big(\boldsymbol{\psi}(\boldsymbol{r},t) - \tau\partial_t\boldsymbol{\psi}(\boldsymbol{r},t) + \mathcal{O}(\tau^2)\Big) \\ &= \tau\partial_t\boldsymbol{\psi}(\boldsymbol{r},t) + \mathcal{O}(\tau^2). \end{aligned} \tag{3.3}$$

We neglect $\mathcal{O}(\tau^2)$ terms and apply the approximation (3.3) on Eq. (3.2). After rearranging terms, this yields:

$$\begin{aligned}(1-\alpha\tau)\partial_t\boldsymbol{\psi} &= \boldsymbol{F}[\boldsymbol{\psi}] \\ \Leftrightarrow \partial_t\boldsymbol{\psi} &= \frac{1}{1-\alpha\tau}\boldsymbol{F}[\boldsymbol{\psi}]\end{aligned} \tag{3.4}$$

Note that the change of the system variable $\partial_t\boldsymbol{\psi}$ becomes infinitely fast when approaching $\alpha\tau = 1$ and has opposite signs for $\alpha\tau < 1$ and $\alpha\tau > 1$. This implies a change of stability, which can be understood as follows:
Consider an uncontrolled system in which the system state is attracted to or repelled from a certain solution. As the sign of the growth rate $\partial_t\boldsymbol{\psi}$ can be changed by time delayed feedback, in principle one can turn attraction into repulsion and vice versa and thereby change the stability of the system state.

If the state $\boldsymbol{\psi}$ is stable (unstable) for $\alpha\tau < 1$ and unstable (stable) for $\alpha\tau > 1$, it must be neutrally stable at $\alpha\tau = 1$. For future reference, we want to put emphasis on the following *distinction between two cases of neutral stability*:

- If neutral stability only occurs for certain parameter values, e.g. $\alpha\tau = 1$, it is related to criticality as a result of a change of stability. These special parameter values $\alpha\tau = 1$ define a neutral stability curve $\tau(\alpha) = \alpha^{-1}$ on which the system dynamics changes qualitatively by a bifurcation.
- If the occurring neutral stability arises for all parameters values, it is a result of symmetry properties. Relating this to the above case, neutral stability occurs not only for parameters which lie on a curve, but for all parameter values in control parameter space. For instance, this was observed for the solutions of the Swift–Hohenberg equation, which are always neutrally stable with respect to spatial translations as a result of translation symmetry.

It is interesting to note that in the limit of small delay times τ, one obtains only one curve at which the stability of a system state changes, regardless of its linear stability analysis and regardless of which eigenmode of the system is considered.

When performing a linear stability analysis, one can analyze under which conditions any of the eigenmodes becomes unstable and derive neutral stability curves for them. As we only obtained one curve, namely $\alpha\tau = 1$, or $\tau(\alpha) = \alpha^{-1}$, within the limit of small delay times τ, the question arises if the change of stability of all eigenmodes is captured by this one curve (within the limit of small τ), or if it only holds for certain eigenmodes, if at all. It will be shown that, although not being equal, all change of stability curves of the eigenmodes approach $\alpha\tau = 1$ in the limit of small τ.

3.2.1 Time Constants and Delay–Induced Adiabatic Elimination

We observed that the change of the system variable $\partial_t\psi$ will be infinitely fast for $\alpha\tau \to 1$ and therefore immediately respond to changes, as can be seen from Eq. (3.4). To understand and interpret the infinitely fast response for $\alpha\tau = 1$, it is instructive to consider the concept of time constants.

Usually, time constants arise in multi–component systems, for example in the two component system:

$$T_u \partial_t u = F(u, v),$$
$$T_v \partial_t v = G(u, v).$$

The factors[1] T_u and T_v are called the time constants or relaxation times of components u and v, respectively. They represent the relative time scales of the components u and v and are a measure how fast the corresponding component responds to changes. The limit $T_i \to 0$ is called an *adiabatic elimination* of the variable $i \in \{u, v\}$ and is related to an instantaneous response of this component.

For the TDF control, one can identify a time constant which depends on the delay control parameters α and τ, and which is introduced by the TDF control mechanism. To do this, we consider the one component system for the time evolution of a variable v

$$T_v \partial_t v = f(v), \tag{3.5}$$

and compare it to Eq. (3.4). Thereby, we obtain

$$T_\psi(\alpha, \tau) = 1 - \alpha\tau. \tag{3.6}$$

[1] Time can be rescaled to set one of the constants to one, e.g. $T_u = 1$, and thereby the other time constant becomes the fraction of both time constants of the unscaled case.

It is interesting to note that this time constant not only depends on delay control parameters, but also can change its sign. For the same reason as stated for $\partial_t \boldsymbol{\psi}$ in Eq (3.4), it can be seen that the sign change of the time constant T_ψ corresponds to a change of stability. Furthermore, the infinitely fast response is described by a vanishing time constant $T_\psi = 0$ at $\alpha\tau = 1$ and involves a delay–induced adiabatic elimination. To show this explicitly, we split

$$T_\psi = |T_\psi| \cdot \mathrm{sign}(T_\psi) = |1 - \alpha\tau| \cdot \mathrm{sign}(1 - \alpha\tau)$$

and rewrite Eq. (3.4) as

$$\begin{aligned} T_\psi \, \partial_t \boldsymbol{\psi} &= \boldsymbol{F}[\boldsymbol{\psi}], \\ \Leftrightarrow |T_\psi| \, \partial_t \boldsymbol{\psi} &= \mathrm{sign}(T_\psi) \cdot \boldsymbol{F}[\boldsymbol{\psi}], \end{aligned} \tag{3.7}$$

where we used $\mathrm{sign}(T_\psi)^{-1} = \mathrm{sign}(T_\psi)$ and in which we can observe that a sign change of T_ψ reverses stability.

3.2.2 Evidence of Spontaneous Symmetry Breaking at $\alpha\tau = 1$

When analyzing the limit of small delay times τ for general systems subjected to scalar TDF, one finds that the stability changes at $\alpha\tau = 1$, but the analysis does not provide information about the scope of this result. It does not indicate if it also arises for other situations and if yes in which. However, there is evidence that $\alpha\tau = 1$, or $\tau(\alpha) = \alpha^{-1}$, may be a *universal curve* for general systems in which symmetry can be *spontaneously broken* in the presence of linear TDF, and can also arise outside the limit of small τ.

For example it was observed for Turing structures in the Lengyel–Epstein model with TDF [ITSO13], for the spontaneous motion of localized structures in the Swift–Hohenberg equation with TDF [TVT+10], as well as for localized structures in a reaction–diffusion system with TDF [Gur13].

All above examples perform a linear stability analysis for an inhomogeneous solution, in which an eigenmode with eigenvalue $\mu = 0$ exists because of translation symmetry. All these references have obtained that the neutrally stable eigenmode of the uncontrolled system state changes its stability when crossing $\alpha\tau = 1$ in control parameter space, thus causing a spontaneous symmetry breaking. The first reference treats this case implicitly and the latter two focus on the eigenvalue $\mu = 0$.

To understand this in general, consider an uncontrolled system state which has a neutrally stable eigenmode with eigenvalue $\mu = 0$ for all parameter values as a result of symmetry, e.g. translation symmetry, and turn on linear time delayed feedback with the control parameters α and τ. Note that TDF does not explicitly break this symmetry. With the application of TDF, the following two scenarios can arise: Either the neutrally stable eigenmode is completely unaffected for all control parameter values, if the symmetry properties are not influenced by TDF and the eigenvalue always remains zero, or the application of TDF allows *spontaneous symmetry breaking*.

In the following analysis, we will prove the occurrence of spontaneous symmetry breaking at $\alpha\tau = 1$ for general systems subjected to linear TDF.

3.3 Linear Stability Problems with TDF: Scalar Coupling

In this section, we perform a linear stability analysis for a system state $\boldsymbol{\psi}^{(0)}$ of a general system subjected to linear TDF with scalar coupling matrices, as given by Eq. (3.2). To do this, we assume[2] the existence of a basis of eigenfunctions for the linearized operator $\underline{\underline{F'}}$.

First, consider the general system without TDF control:

$$\partial_t \boldsymbol{\psi}(\boldsymbol{r}, t) = \boldsymbol{F}(\boldsymbol{\psi}). \tag{3.8}$$

Let $\boldsymbol{\psi}^{(0)}$ be its steady state solution and denote the small perturbation to $\boldsymbol{\psi}^{(0)}$ as $\boldsymbol{\delta\psi}(t)$. The linear stability problem is then given by

$$\partial_t \, \boldsymbol{\delta\psi}(\boldsymbol{r}, t) = \underline{\underline{F'}} \cdot \boldsymbol{\delta\psi}(\boldsymbol{r}, t), \tag{3.9}$$

where $\underline{\underline{F'}}$ is the linearized operator evaluated at the steady state $\boldsymbol{\psi}^{(0)}$.

If $\underline{\underline{F'}}$ is diagonalizable, a basis of eigenvectors or eigenfunctions $\boldsymbol{\varphi}_j$ exists, which is finite dimensional for an ordinary differential equation and infinite dimensional for a partial differential equation. If this basis exists, the general solution of the linear stability problem is given by

$$\boldsymbol{\delta\psi}(\boldsymbol{r}, t) = \sum_j C_j e^{\mu_j t} \boldsymbol{\varphi}_j(\boldsymbol{r}), \tag{3.10}$$

where the μ_j denote the corresponding eigenvalues of eigenfunctions $\boldsymbol{\varphi}_j$ with respect to $\underline{\underline{F'}}$, and C_j are constant amplitudes. The steady state solution $\boldsymbol{\psi}^{(0)}$ is linearly

[2] If this is not the case, one needs to find generalized eigenvectors / eigenfunctions, but this scenario is out of the scope of this thesis. Currently, it is not yet investigated whether the following analysis can be generalized to cope with this scenario.

stable if $\boldsymbol{\delta\psi} \to 0$ and unstable otherwise. In terms of eigenvalues, $\boldsymbol{\psi}^{(0)}$ is stable if all eigenvalues satisfy Re $\mu_j \leq 0$ and unstable if any Re $\mu_j > 0$.

Now consider the scenario of linear time delayed feedback with a scalar coupling matrix $\underline{\underline{K}} = \alpha \cdot \underline{\underline{1}}$, in which $\underline{\underline{K}}$ and $\underline{\underline{F'}}$ commutate for trivial reasons. Then, the eigenfunctions of the problem with delay are the same as the eigenfunctions without delay. For scalar TDF, the controlled system is given by Eq. (3.2) and its linear stability problem with TDF is given by

$$\partial_t \boldsymbol{\delta\psi}(\boldsymbol{r}, t) = \underline{\underline{F'}}\, \boldsymbol{\delta\psi}(\boldsymbol{r}, t) + \alpha \cdot \underline{\underline{1}} \left(\boldsymbol{\delta\psi}(\boldsymbol{r}, t) - \boldsymbol{\delta\psi}(\boldsymbol{r}, t - \tau)\right), \tag{3.11}$$

where $\underline{\underline{F'}}$ is the linearized operator evaluated at the steady state $\boldsymbol{\psi}^{(0)}$.

By assumption, there exists a basis of eigenfunctions $\boldsymbol{\varphi}_j$ of $\underline{\underline{F'}}$ with corresponding eigenvalues μ_j, which allows to make the following ansatz for the perturbation $\boldsymbol{\delta\psi}$ in the presence of TDF

$$\boldsymbol{\delta\psi} = \sum_j C_j e^{\lambda_j t} \boldsymbol{\varphi}_j. \tag{3.12}$$

Here, λ_j are the yet unknown eigenvalues of the linear stability problem with TDF with scalar coupling matrices, and C_j are constant amplitudes. Substituting this ansatz in Eq. (3.11) yields:

$$\begin{aligned} \sum_j C_j \lambda_j e^{\lambda_j t} \boldsymbol{\varphi}_j &= \sum_j C_j \left[e^{\lambda_j t} \underline{\underline{F'}} + \alpha \cdot \underline{\underline{1}} \left(e^{\lambda_j t} - e^{\lambda_j (t-\tau)} \right) \right] \boldsymbol{\varphi}_j & (3.13) \\ &= \sum_j C_j \left[e^{\lambda_j t} \mu_j + \alpha \cdot \underline{\underline{1}} \left(e^{\lambda_j t} - e^{\lambda_j (t-\tau)} \right) \right] \boldsymbol{\varphi}_j & (3.14) \end{aligned}$$

Since the eigenfunctions $\boldsymbol{\varphi}_j$ build a basis, they are linearly independent and one can compare coefficients of the above equation. This yields a solvability condition for the ansatz (3.12):

$$\boxed{\lambda_j = \mu_j + \alpha \left(1 - e^{-\lambda_j \tau}\right)} \tag{3.15}$$

Equation (3.15) determines the eigenvalues λ_j of the linear stability problem with time delayed feedback and is called the **characteristic equation**. It links the eigenvalues of the stability problem with TDF, denoted as λ_j, to the eigenvalues of the stability problem without TDF, denoted as μ_j.

It is interesting to note the *self–similarity of linear TDF*: The same characteristic equation arises for every eigenvalue μ_j of the uncontrolled system state.

3.4 Solutions of the Characteristic Equation

We solve the characteristic equation (3.15) for the eigenvalues λ_j of the stability problem with TDF. This can be done in terms of the Lambert–W function [CGH+96], which is the multi–valued inverse of the function ze^z, $z \in \mathbb{C}$. First, we solve the characteristic equation for λ_j and then give a brief introduction to the Lambert–W function, which covers the relevant details for our further analysis. For an extensive review, refer to Ref. [CGH+96].

The characteristic equation (3.15) can be rearranged to

$$\{(\lambda_j - \mu_j - \alpha)\tau\}\, e^{\{(\lambda_j - \mu_j - \alpha)\tau\}} = -\alpha\tau e^{-(\mu_j+\alpha)\tau}, \tag{3.16}$$

where the left hand side is of the form ze^z with $z = (\lambda_j - \mu_j - \alpha)\tau$. Applying the Lambert–W function and solving for the eigenvalues λ_j of the linear stabilty problem with TDF yields

$$\boxed{\lambda_j(n, \mu_j, \alpha, \tau) = \mu_j + \alpha + \frac{1}{\tau} W_n\left(-\alpha\tau e^{-(\mu_j+\alpha)\tau}\right), \quad n \in \mathbb{Z},} \tag{3.17}$$

where n is the branch index of the Lambert–W function. As usual, the real part Re λ_j specifies the growth rate of perturbations and the imaginary part Im λ_j determines its oscillation frequency.

Note that every eigenvalue μ_j of the linear stability problem without TDF induces an infinite number of eigenvalues $\lambda_j(n)$, $n \in \mathbb{Z}$ of the stability problem with TDF. This is a consequence of the aforementioned infinite dimensional phase space [Hal93] for delay differential equations. To sum up, the solution for the ansatz (see Eq. (3.12)) we made for the perturbation $\boldsymbol{\delta\psi}$ of the linear stability analysis with TDF reads:

$$\boxed{\boldsymbol{\delta\psi} = \sum_j \sum_n C_j e^{\lambda_j(n,\mu_j,\alpha,\tau)\cdot t} \boldsymbol{\varphi}_j.} \tag{3.18}$$

In the limit $\alpha \to 0$ or $\tau \to 0$, the TDF control term vanishes, which can also be observed for the eigenvalues $\lambda_j(n, \mu_j, \alpha, \tau)$:

$$\lim_{\substack{\alpha\to 0\\ \tau\to 0}} \lambda_j(n, \mu_j, \alpha, \tau) = \begin{cases} \mu_j & n = 0 \\ -\infty & n \neq 0 \end{cases}. \tag{3.19}$$

As expected by physical intuition, in the limit of vanishing TDF control, only one of the infinite number of branches persists and the infinite sum

$$\lim_{\substack{\alpha\to 0\\ \tau\to 0}} \sum_n e^{\lambda_j(n,\mu_j,\alpha,\tau)t} = e^{\mu_j t}$$

reduces to the element with the eigenvalue μ_j of the uncontrolled system. Details of taking this limit will be explained when discussing the Lambert–W function in section 3.4.1.

Furthermore, in order to understand how the stability of $\boldsymbol{\psi}^{(0)}$ is influenced by TDF, it is instructive to consider the reverse situation:
Regard an uncontrolled system state as a system state to which a vanishing TDF control is applied, i.e., $\alpha = 0$ or $\tau = 0$ holds. Consider an eigenvalue μ of this uncontrolled system state, and apply TDF control by varying α and τ. When applying TDF, an infinite number of branches $n \in \mathbb{Z}$ arises due to the infinite dimensionality of phase space of delay differential equations [Hal93]. One of these branches, namely $n = 0$, starts at μ, while the other infinite number of branches $n \in \mathbb{Z} \setminus \{0\}$ start at $-\infty$, all belonging to the same eigenvalue μ.

Initially, all branches $n \neq 0$ are on the left half–plane of the complex plane, and the branch $n = 0$ is on the

$$\begin{aligned} \text{left half–plane,} \quad & \text{if Re } \mu \leq 0, \\ \text{right half–plane,} \quad & \text{if Re } \mu \geq 0. \end{aligned}$$

When varying TDF control parameters, the eigenvalues $\lambda(n, \mu, \alpha, \tau)$ may switch their half–plane for certain parameter values, thus causing a bifurcation.

To understand the infinite number of branches and other properties of our solution, we give a brief introduction to the Lambert–W function, which covers the multi–valuedness, the near–conjugate symmetry and its behaviour in complex plane.

3.4.1 The Lambert–W Function

The Lambert–W function [CGH+96] is defined as the multi–valued inverse of ze^z, $z \in \mathbb{C}$, where the multi–valuedness results from ze^z being non–injective.

To illustrate this multi–valuedness, consider the function ze^z, $z \in \mathbb{C}$, and represent the first complex factor as $z = |z|e^{i\phi_z}$ and the latter as $z = z_\mathrm{R} + iz_\mathrm{I}$:

$$\begin{aligned} ze^z &= |z|e^{i\phi_z}e^{z_R + iz_I} \\ &= |z|e^{z_R}e^{i(\phi_z + z_I)} \end{aligned} \tag{3.20}$$

We can identify the phase of the complex number ze^z as $\phi_z + z_\mathrm{I}$. Since only values of the phase modulo 2π are relevant, ranges of phase values $\phi_z + z_\mathrm{I}$ from different intervals

$$2\pi \cdot [n, n+1],\ n \in \mathbb{Z}$$

are mapped to the same complex number ze^z. This results in different branches n that belong to these intervals, when considering the inverse of $z \to ze^z$.

Furthermore, the branches of the Lambert–W function have *near–conjugate symmetry* [CGH+96], which for the case of real–valued z can be interpreted as follows: Every non–real branch of $W_n(z)$ has a corresponding conjugate branch and these branches build *near–conjugate branch pairs*. For details on the general case, refer to Ref. [CGH+96].

Except for $n = 0$ and $n = -1$, all branches n of $W_n(z)$ are always complex, and $W_0(z)$ and $W_1(z)$ are only real for certain ranges of z. The real–valued case for ze^z and $W_n(z)$ vs. z is shown in Fig. 3.1 and the complex–valued cases are shown in Fig. 3.2 and 3.3. Figure 3.2 shows the real and imaginary part of $W_n(z)$ vs. z and Fig. 3.3 shows $W_n(z)$ in the complex plane. It can be seen that at $z = 0$,

$$\lim_{z \to 0} \text{Re } W_n(z) = \begin{cases} 0 & n = 0 \\ -\infty & n \neq 0 \end{cases}$$

and that the imaginary part has a jump–discontinuity, at which the pairing of the corresponding near–conjugate branch pairs shifts by one element.

Note that in general

$$W_n(ze^z) \neq z. \tag{3.21}$$

This only holds for the branch n in which the phase of ze^z, namely $\phi_z + z_i$, lies within the aforementioned interval $2\pi[n, n+1]$.

3.4.2 Neutral Stability Curves

Our goal is to solve the characteristic equation (3.15) for the neutral stability curves $\tau_c(\alpha)$, at which the stability of the eigenmode $\boldsymbol{\varphi}_j$ changes. To this end, we consider the delay strength α as a parameter and solve (3.15) for the delay time $\tau = \tau_c(\alpha)$ at which the corresponding eigenvalue λ_j crosses the imaginary axis in the complex plane, thereby changing the sign of its growth rate Re λ_j. Crossing the neutral stability curves $\tau_c(\alpha)$ in control parameter space leads to a bifurcation of the system state $\boldsymbol{\psi}^{(0)}$. They can be determined by the condition:

$$\text{Re } \lambda_j(n, \mu_j, \alpha, \tau_c(\alpha)) = 0. \tag{3.22}$$

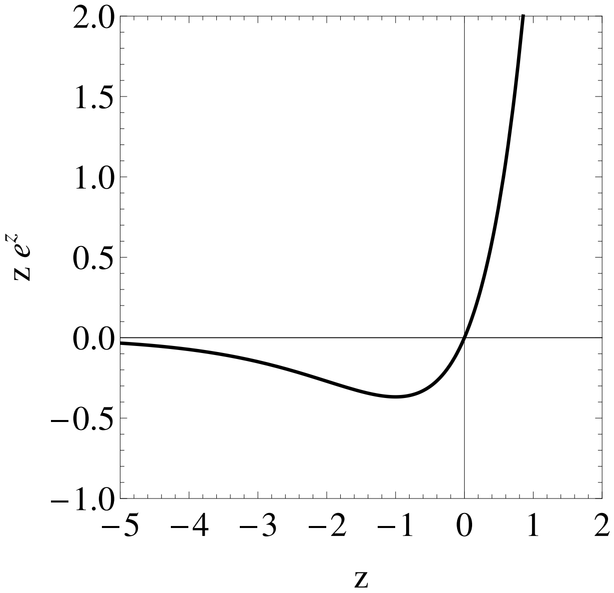

(a)

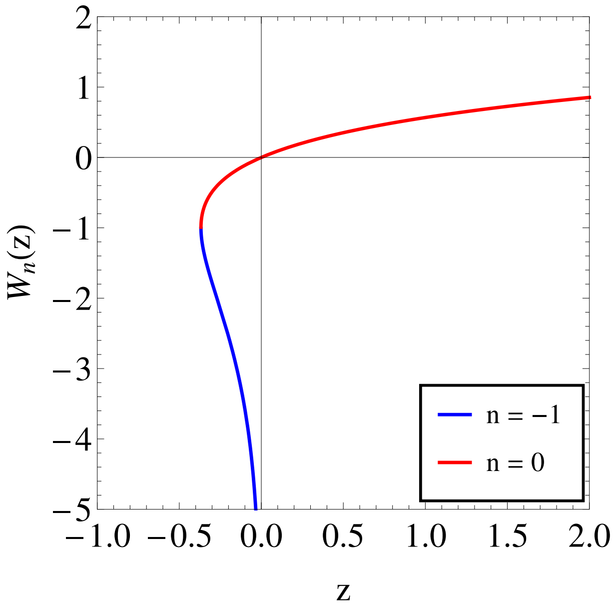

(b)

Figure 3.1: Real–valued function ze^z and its inverse $W_n(z)$ on the real line. a) ze^z vs. z for $z \in \mathbb{R}$. b) $W_n(z)$ vs. z for the two real branches $n = 0$ and $n = -1$. Inverting ze^z results in a split at the minimum $(-1, -e^{-1})$, which becomes the so–called branch point of W_n, at which both branches intersect. The diagram only shows ranges of z for which the W_n are real–valued.

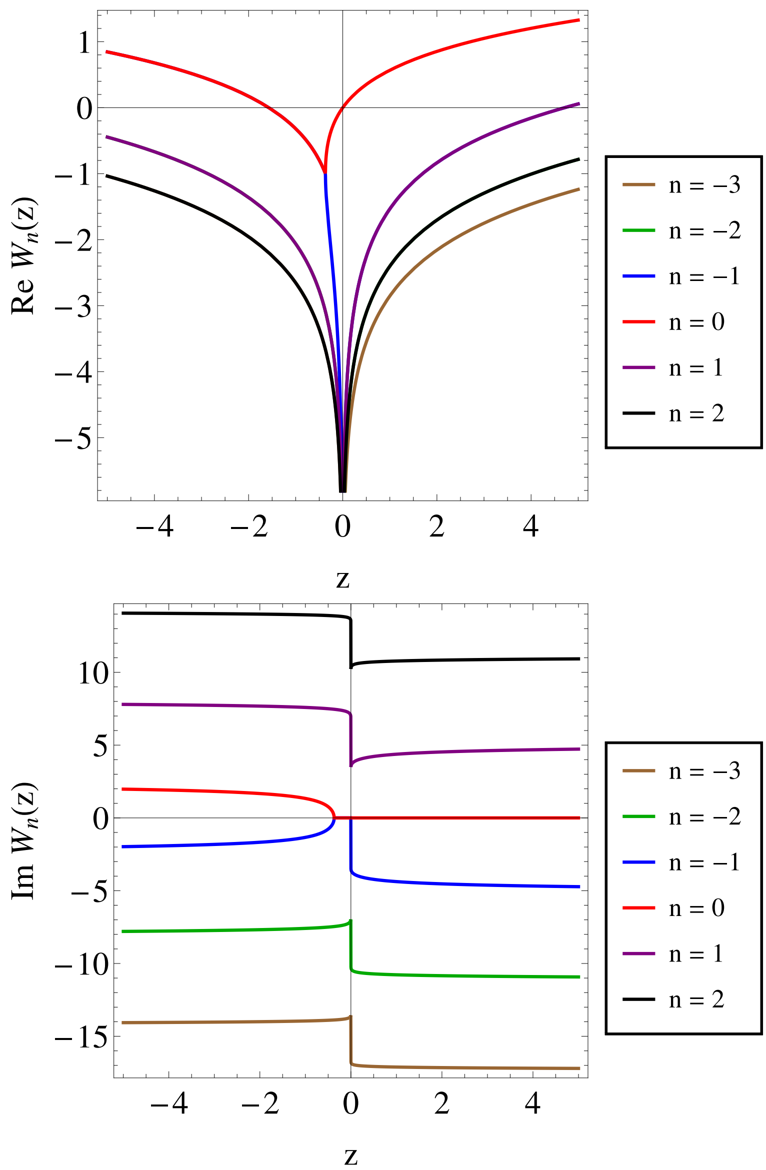

Figure 3.2: Real and imaginary parts of $W_n(z)$ for the branches $-3 \leq n \leq 2$. Corresponding near–conjugate branch pairs have the same real part, whereas their imaginary parts have opposite signs. The pairing of near–conjugate branch pairs shifts by one element due to a jump–discontinuity at $z = 0$.

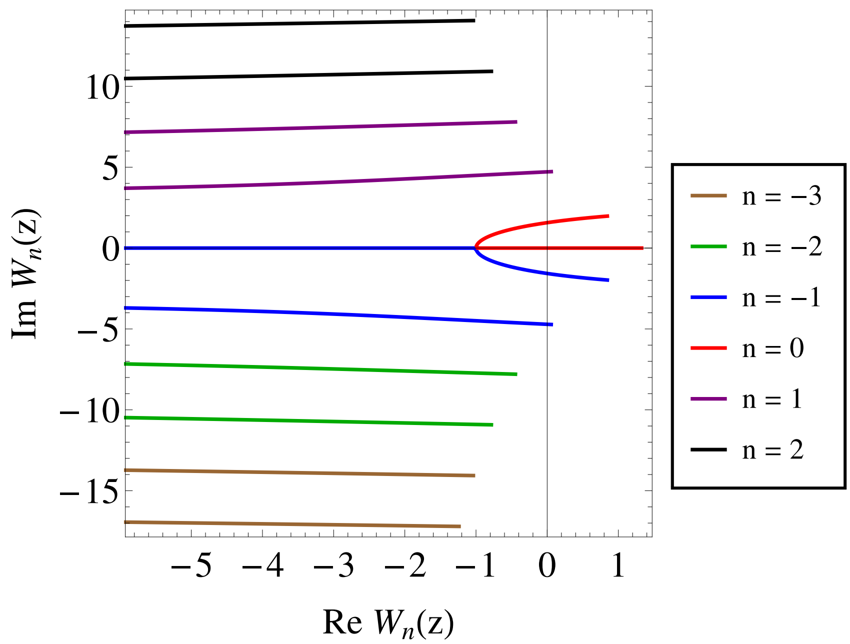

Figure 3.3: Complex plane representation of the complex–valued $W_n(z)$ for the branches $-3 \leq n \leq 2$ and $z \in [-5, 5]$. The upper edge of each curve belongs to -5 , and the lower edge belongs to $+5$. This can be concluded, since at the jump–discontinuity the imaginary part jumps downwards. In comparison with Fig. 3.2, one can observe that when z crosses $z = 0$, the real parts of branches with branch index $n \neq 0$ have a singularity and go to $-\infty$ and their imaginary parts have a jump–discontinuity at which the pairing of the corresponding near–conjugate branch pairs shifts by one element. The branches $n = 0$ and $n = -1$ intersect at the branch point, where both branches change from real– to complex–valuedness.

Since there is an infinite number of branches of eigenvalues $\lambda_j(n)$, $n \in \mathbb{Z}$, one obtains neutral stability curves that depend on the branch index. The stability of $\boldsymbol{\varphi}_j$ changes, if the TDF control parameters (α, τ) can be chosen, such that

$$\tau > \tau_c(\alpha). \tag{3.23}$$

We analytically derive the neutral stability curves $\tau_c(\alpha)$ for the general case of complex–valued $\mu \in \mathbb{C}$, and their associated oscillation frequency $\mathrm{Im}\ \lambda_j$ on the neutral stability curve. The implicit equation for the neutral stability curves has been recently obtained in [Gur14]. Our goal is to explicitly solve it and derive properties of the solution. Note that the eigenvalues λ of the linear stability problem with TDF can also be complex, even if $\mu \in \mathbb{R}$, because of the properties of the Lambert–W function.

For convenience, we drop the index j of μ_j, λ_j and $\boldsymbol{\varphi}_j$, since all eigenvalues satisfy the same equation and the following analysis holds for each of them. Then, the characteristic equation (3.15) becomes

$$\lambda = \mu + \alpha\left(1 - e^{-\lambda\tau}\right). \tag{3.24}$$

One can obtain the neutral stability curves $\tau_c(\alpha)$ and the oscillation frequency $\mathrm{Im}\ \lambda$ on the neutral stability curve as follows: The eigenvalue $\lambda = \sigma + i\omega$ and the characteristic equation (3.15) are split into their real and imaginary parts:

$$\sigma = \mathrm{Re}\ \mu + \alpha - \alpha e^{-\sigma\tau}\cos(\omega\tau) \tag{3.25a}$$

$$\omega = \mathrm{Im}\ \mu + \alpha e^{-\sigma\tau}\sin(\omega\tau) \tag{3.25b}$$

Setting $\sigma = 0$ and rearranging terms yields

$$\cos(\omega\tau) = \frac{\mathrm{Re}\ \mu + \alpha}{\alpha}, \tag{3.26a}$$

$$\omega = \mathrm{Im}\ \mu + \alpha\sin(\omega\tau). \tag{3.26b}$$

Solve for oscillation frequency ω:
Rearranging Eq. (3.26a) for $\omega\tau$

$$\omega\tau = \begin{cases} \pm\mathrm{arccos}\left(\frac{\mathrm{Re}\ \mu+\alpha}{\alpha}\right) + 2\pi m, \quad m \in \mathbb{Z}, & \text{if } \left|\frac{\mathrm{Re}\ \mu+\alpha}{\alpha}\right| \leq 1 \\ \text{undefined} & \text{else} \end{cases} \tag{3.27}$$

and substituting it in Eq. (3.26b) yields:

$$\omega = \mathrm{Im}\ \mu + \alpha\sin\left(\pm\mathrm{arccos}\left(\frac{\mathrm{Re}\ \mu + \alpha}{\alpha}\right) + 2\pi m\right), \quad m \in \mathbb{Z}. \tag{3.28}$$

By applying trigonometric identities, we obtain the oscillation frequency ω on the neutral stability curve:

$$\boxed{\omega = \begin{cases} \pm\alpha\sqrt{1-\left(\frac{\text{Re }\mu+\alpha}{\alpha}\right)^2} + \text{Im }\mu & \text{if } \left|\frac{\text{Re }\mu+\alpha}{\alpha}\right| \leq 1 \\ \text{undefined} & \text{else} \end{cases}} \tag{3.29}$$

Solve for neutral stability curve $\tau_c(\alpha)$:
Combining equations (3.27) and (3.29) yields

$$\pm\arccos\left(\frac{\text{Re }\mu+\alpha}{\alpha}\right) + 2\pi m = \pm\alpha\tau\sqrt{1-\left(\frac{\text{Re }\mu+\alpha}{\alpha}\right)^2} + \tau\ \text{Im }\mu, \tag{3.30}$$

which can be solved for the neutral stability curve $\tau = \tau_c(\alpha)$:

$$\boxed{\tau_c(m,\mu,\alpha) = \begin{cases} \dfrac{\arccos\left(\frac{\text{Re }\mu+\alpha}{\alpha}\right)\pm 2\pi m}{\alpha\sqrt{1-\left(\frac{\text{Re }\mu+\alpha}{\alpha}\right)^2}\pm\text{ Im }\mu} & \text{if } \left|\frac{\text{Re }\mu+\alpha}{\alpha}\right| \leq 1 \\ \text{undefined} & \text{else} \end{cases}} \tag{3.31}$$

where we divided by the $\pm$ sign and rearranged terms.

Although this is a mathematically allowed solution for all m and both cases of $\pm$, the index m and the $\pm$ cases have to be adapted accordingly to ensure a physically correct solution. Due to causality, the delay time τ and $\tau_c(\alpha)$ have to be positive, and therefore the nominator and the denominator of Eq. (3.31) must have the same sign.

For the indices m for which this physical requirement can be satisfied, a neutral stability curve exists and the stability of the corresponding branch changes when crossing this curve in control parameter space.

It is unclear how the $\pm m$ in the neutral stability curves are related to the branch index n of our eigenvalues $\lambda(n)$ for complex $\mu \in \mathbb{C}$, whereas they can be related for $\mu \in \mathbb{R}$. For notational convenience, we eliminate the sign in $\pm 2\pi m$ in the neutral stability curves, by defining a new index $\widetilde{m}$ by $m = \pm\text{sign}(\alpha)\widetilde{m}$. It turns out that the index $\widetilde{m}$ is the index of conjugate branch pairs of the Lambert–W function, which can be understood as follows: Consider the argument z which is supplied to the Lambert–W function in the eigenvalues λ:

$$\lambda = \mu + \alpha + \frac{1}{\tau}W_n(\underbrace{-\alpha\tau e^{(\mu+\alpha)\tau}}_{=:z})$$

For $\mu \in \mathbb{R}$, z has the opposite sign of α. Comparing this to Fig. 3.2, we see that for ($\alpha < 0 \leftrightarrow z > 0$) the pairing of conjugate branches is $\widetilde{m} = \pm n$ and for ($\alpha > 0 \leftrightarrow z < 0$) the pairing is ($\widetilde{m} = 0 \leftrightarrow n = 0, -1$), ($\widetilde{m} = 1 \leftrightarrow n = 1, -2$), etc. The above asymmetry arises since the pairing of corresponding near–conjugate branch pairs of the Lambert–W function shifts by one element when crossing $W_n(0)$.

The solvability condition

When solving for the neutral stability curves $\tau_c(\alpha)$ and the oscillation frequency $\omega := \mathrm{Im}\ \lambda$ on the neutral stability curve, we encountered that the solution only exists, if

$$\left|\frac{\mathrm{Re}\ \mu + \alpha}{\alpha}\right| = \left|\frac{\mathrm{Re}\ \mu}{\alpha} + 1\right| \leq 1. \tag{3.32}$$

This solvability condition specifies under which condition a change of stability can occur in the presence of TDF. Rearranging it yields:

$$\begin{aligned} &\left[\frac{\mathrm{Re}\ \mu}{\alpha} + 1 \leq 1\right] \wedge \left[\frac{\mathrm{Re}\ \mu}{\alpha} + 1 \geq -1\right] \\ \Leftrightarrow &\left[\frac{\mathrm{Re}\ \mu}{\alpha} \leq 0\right] \wedge \left[\frac{\mathrm{Re}\ \mu}{\alpha} \geq -2\right] \\ \Leftrightarrow &\underbrace{[\mathrm{sign}(\mathrm{Re}\ \mu) \cdot \mathrm{sign}(\alpha) = -1]}_{=:\ \mathrm{I}} \wedge \underbrace{\left[|\alpha| \geq \frac{-\mathrm{sign}(\alpha) \cdot \mathrm{Re}\ \mu}{2} = \frac{|\mathrm{Re}\ \mu|}{2}\right]}_{=:\ \mathrm{II}} \end{aligned}$$

Term I specifies that in order to get a stability change, the delay strength α and the real part of eigenvalue μ_j of the uncontrolled system state must have opposite signs, which specifies how the delay strength α has to be chosen:

$$\begin{aligned} &\text{stabilization scenario:} && \mathrm{Re}\ \mu > 0,\ \alpha \leq 0, \\ &\text{destabilization scenario:} && \mathrm{Re}\ \mu \leq 0,\ \alpha \geq 0. \end{aligned} \tag{3.33}$$

Term II determines the minimum delay strength for a stability change:

$$|\alpha| \geq \frac{|\mathrm{Re}\ \mu|}{2}. \tag{3.34}$$

Spontaneous symmetry breaking at $\alpha\tau = 1$

Relating to the evidence of spontaneous symmetry breaking at $\alpha\tau = 1$ (see section 3.2.2), the question arises, if the obtained neutral stability curves $\tau_c(\alpha)$ include this special case. Therefore, we consider an uncontrolled system state which has an eigenmode with corresponding eigenvalue $\mu = 0$ as a result of symmetry, and turn on TDF. When crossing the neutral stability curve, if it exists, the corresponding eigenmode becomes unstable and the symmetry is spontaneously broken. To investigate this, we take the limit $\mu \to 0$ of Eq. (3.31):

$$\begin{aligned}
\lim_{\mu\to 0} \tau_c(m,\mu,\alpha) &= \lim_{\mu\to 0} \begin{cases} \frac{\arccos\left(\frac{\text{Re } \mu+\alpha}{\alpha}\right)\pm 2\pi m}{\alpha\sqrt{1-\left(\frac{\text{Re } \mu+\alpha}{\alpha}\right)^2}\pm \text{ Im } \mu} & \text{if } \left|\frac{\text{Re } \mu+\alpha}{\alpha}\right| \leq 1 \\ \text{undefined} & \text{else} \end{cases} \\
&= \begin{cases} \frac{1}{\alpha} & \text{if } m = 0 \\ \infty & \text{if } m \neq 0 \end{cases}, \qquad (3.35)
\end{aligned}$$

where we applied l'Hôpital's rule to take the limit. The case differentiation can be dropped, since the solvability condition is always satisfied for $\mu = 0$, since $\lim_{\mu\to 0} \left|\frac{\text{Re } \mu+\alpha}{\alpha}\right| = 1 \leq 1$.

To sum up, the eigenmode with eigenvalue $\mu = 0$ in the uncontrolled system state loses its stability if $\tau > \tau_c(\alpha) = \alpha^{-1}$, since the branch with index $m = 0$ crosses the imaginary axis, thus destabilizing this eigenmode. Thereby, we demonstrated that symmetry is spontaneously broken at $\alpha\tau = 1$ for a general system subjected to linear TDF with scalar coupling matrices.

Oscillation frequency ω at the bifurcation
Consider the oscillation frequency ω in Eq. (3.29). Since the solvability condition guarantees that $\left(\frac{\text{Re } \mu+\alpha}{\alpha}\right)^2 \leq 1$, the oscillation frequency ω on the neutral stability curve reads:

$$\omega = \text{Im } \mu, \quad \text{if Re } \mu = 0 \qquad (3.36)$$

$$\omega \neq \text{Im } \mu, \quad \text{if Re } \mu \neq 0 \qquad (3.37)$$

It can be observed that the oscillation frequency ω at the delay–induced bifurcation is the same as the oscillation frequency Im μ of the uncontrolled system, if the eigenvalue μ of the uncontrolled system lies on the imaginary axis in the complex plane, and that they differ otherwise.

For an eigenmode $\boldsymbol{\varphi}$ with real–valued eigenvalue $\mu \in \mathbb{R}$, the oscillation frequency is zero, i.e., Im $\mu = 0$, and one obtains:

$$\omega = 0 \quad \text{if Re } \mu = 0, \qquad (3.38)$$

$$\omega \neq 0, \quad \text{if Re } \mu \neq 0, \qquad (3.39)$$

Since the oscillation frequency of the eigenmode is zero by assumption, at the change of stability, one obtains a TDF–induced oscillation frequency ω for all eigenvalues

$\mu \neq 0$, whereas the frequency is zero, if the eigenvalue μ is zero.

On the one hand, this means that neutrally stable eigenmodes with corresponding eigenvalue $\mu = 0$ lose stability in a bifurcation which is of not oscillatory type, i.e. the growth of the perturbation is monotonous in time. On the other hand, this states that all stable eigenmodes with corresponding eigenvalue $\mu < 0$ lose stability in a bifurcation of oscillatory type.

For future reference, we underline that eigenvalues $\mu = 0$ belong to eigenmodes $\boldsymbol{\varphi}$ which represent symmetry operations. If the eigenvalue $\mu = 0$ changes stability, the corresponding perturbation grows monotonously in time and breaks the symmetry. We shall see that for the Swift-Hohenberg equation with TDF, this situation arises and creates a drift bifurcation which breaks the translational symmetry.

3.4.3 Implications for Real–Valued μ

We can show that for systems whose linear stability problem with TDF is governed by the characteristic equation (3.15), system states with real–valued eigenvalues $\mu \in \mathbb{R}$ can be destabilized, but not stabilized.

For Im $\mu = 0$, the neutral stability curves (see Eq. (3.31)) become:

$$\tau_c(m,\mu,\alpha) = \begin{cases} \frac{\arccos\left(\frac{\mathrm{Re}\,\mu+\alpha}{\alpha}\right)\pm 2\pi m}{\alpha\sqrt{1-\left(\frac{\mathrm{Re}\,\mu+\alpha}{\alpha}\right)^2}} & \text{if } \left|\frac{\mathrm{Re}\,\mu+\alpha}{\alpha}\right| \leq 1 \\ \text{undefined} & \text{else} \end{cases} \tag{3.40}$$

We rewrite the case for which it is defined, by factoring out the sign(α):

$$\tau_c(m,\mu,\alpha) = \frac{\mathrm{sign}(\alpha)\left[\arccos\left(\frac{\mathrm{Re}\,\mu+\alpha}{\alpha}\right) \pm 2\pi m\right]}{|\alpha|\sqrt{1-\left(\frac{\mathrm{Re}\,\mu+\alpha}{\alpha}\right)^2}}.$$

Note that $\tau_c > 0$ must hold due to causality and that the range of $\arccos(z) \in [0, \pi]$. Since the denominator is positive, the nominator must be positive, which yields:

- For the destabilization scenario ($\mu < 0$, $\alpha > 0$), the solution exists for all m by choosing the correct sign out of $\pm$; all branches start on the left half–plane of the complex plane and change half–plane when $\tau > \tau_c$.
- For the case ($\mu > 0$, $\alpha < 0$), the solution only exists for $m \neq 0$, that is the branches starting from $-\infty$ on the left half–plane can change half–planes, which would lead to a destabilization, but the branch with $m = 0$, which starts

at $\mu > 0$, never changes half–planes. It can be observed, that the eigenvalue approaches the imaginary axis, but it never crosses it.

Therefore, a stabilization of eigenmodes with eigenvalue $\mu \in \mathbb{R}_+$ is impossible with the chosen type of TDF control in Eq. (3.2), whereas complex eigenvalues $\mu \in \mathbb{C}$ with positive real part can be stabilized, as seen in Ref. [Gur14]. Fig. 3.4 shows a representative example of neutral stability curves for the destabilization of stable eigenmode with negative eigenvalue $\mu = -1$.

A given system state $\boldsymbol{\psi}^{(0)}$ is destabilized, if any of its eigenmodes becomes unstable. The critical delay time τ_u at which the first eigenmode becomes unstable is given by the first curve which is crossed in control parameter space when varying α and τ, which is reflected by

$$\boxed{\tau_u(\alpha) = \min_{m,\mu} \tau_c(m, \mu, \alpha).} \tag{3.41}$$

3.5 Linear Stability Problems with TDF: Non–Scalar Coupling

In this section, we perform a linear stability analysis for a system state $\boldsymbol{\psi}^{(0)}$ in a general system subjected to linear TDF with non–scalar coupling matrices $\underline{\underline{K}}$. The following analysis is based on the assumption that the coupling matrix $\underline{\underline{K}}$ and the linearized operator $\underline{\underline{F'}}$ commutate.

As usual, we denote the steady state solution of the general system without TDF control

$$\partial_t \boldsymbol{\psi}(\boldsymbol{r}, t) = \boldsymbol{F}(\boldsymbol{\psi}) \tag{3.42}$$

as $\boldsymbol{\psi}^{(0)}$, and denote the small perturbation to $\boldsymbol{\psi}^{(0)}$ as $\boldsymbol{\delta\psi}(\boldsymbol{r}, t)$. The linear stability problem is given by

$$\partial_t \, \boldsymbol{\delta\psi}(\boldsymbol{r}, t) = \underline{\underline{F'}} \cdot \boldsymbol{\delta\psi}(\boldsymbol{r}, t), \tag{3.43}$$

and can be solved in terms of eigenvalues $\mu_j^{F'}$ and eigenfunctions $\boldsymbol{\varphi}_j$ of $\underline{\underline{F'}}$

$$\boldsymbol{\delta\psi} = \sum_j C_j e^{\mu_j^{F'} \cdot t} \boldsymbol{\varphi}_j, \tag{3.44}$$

with constant amplitudes C_j.

Now consider the non–scalar TDF control mechanism, which is given by Eq. (3.1). The corresponding linear stability problem for non–scalar coupling reads:

$$\partial_t \boldsymbol{\delta\psi} = \underline{\underline{F'}} \cdot \boldsymbol{\delta\psi} + \underline{\underline{K}} \left(\boldsymbol{\delta\psi}(\boldsymbol{r}, t) - \boldsymbol{\delta\psi}(\boldsymbol{r}, t - \tau) \right). \tag{3.45}$$

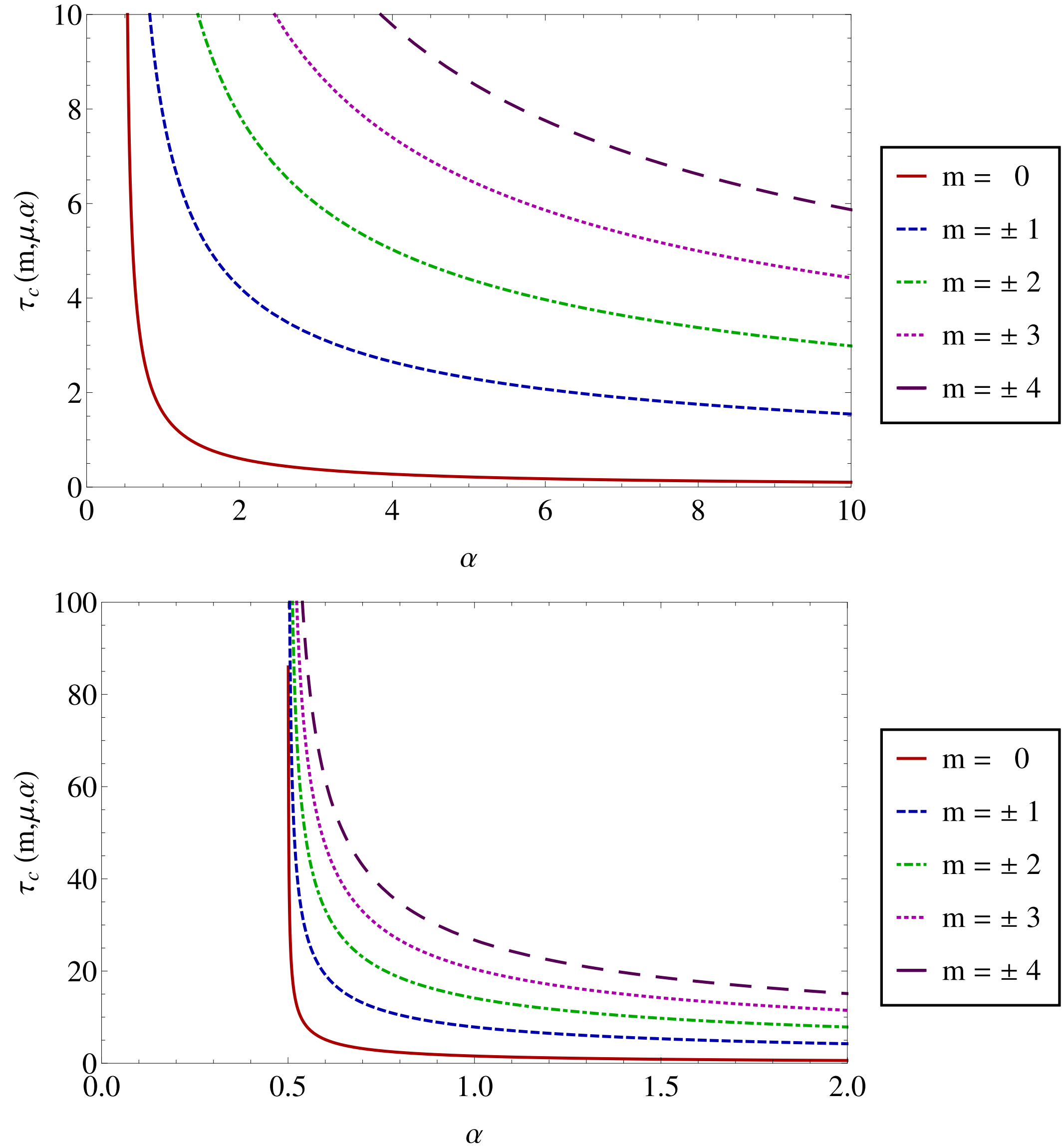

Figure 3.4: Neutral stability curves $\tau_c(m, \mu, \alpha)$ vs. α for fixed $\mu = -1$ and branches $-5 \leq m \leq 5$. The different plotranges illustrate the overall behaviour, and the asymptote at $\alpha_{\text{min}} = \frac{|\text{Re}\,\mu|}{2}$ for all branches m.

We can solve Eq. (3.45), provided that its right hand side can be diagonalized. For this case, $\underline{\underline{F'}}$ and $\underline{\underline{K}}$ have to be simultaneously diagonalizable, which is equivalent to the assumption that $\underline{\underline{F'}}$ and $\underline{\underline{K}}$ commutate. Note that this is a generalization of the case of scalar coupling matrices $\underline{\underline{K}} = \alpha \cdot \underline{\underline{1}}$, in which $\underline{\underline{F'}}$ and $\underline{\underline{K}} = \alpha \cdot \underline{\underline{1}}$ commutated for trivial reasons, since the identity matrix commutates with all matrices.

If they commutate, there exists a common basis of eigenfuctions $\boldsymbol{\varphi}_j$ with corresponding eigenvalues $\mu_j^{F'}$ and μ_j^K of matrices $\underline{\underline{F'}}$ and $\underline{\underline{K}}$, respectively:

$$\underline{\underline{F'}}\,\boldsymbol{\varphi}_j = \mu_j^{F'}\,\boldsymbol{\varphi}_j, \tag{3.46}$$

$$\underline{\underline{K}}\,\boldsymbol{\varphi}_j = \mu_j^{K}\,\boldsymbol{\varphi}_j, \tag{3.47}$$

We change the basis to the eigenbasis of common eigenfunctions $\boldsymbol{\varphi}_j$ by making the ansatz

$$\boldsymbol{\delta\psi} = \sum_j C_j e^{\lambda_j t} \boldsymbol{\varphi}_j, \tag{3.48}$$

where λ_j are the yet unknown eigenvalues of the stability problem with non–scalar TDF. Substituting this ansatz in Eq. (3.45) yields:

$$\sum_j C_j \lambda_j e^{\lambda_j t} \boldsymbol{\varphi}_j = \sum_j C_j \left[e^{\lambda_j t} \underline{\underline{F'}} + \underline{\underline{K}} \left(e^{\lambda_j t} - e^{\lambda_j (t-\tau)} \right) \right] \boldsymbol{\varphi}_j, \tag{3.49}$$

$$= \sum_j C_j \left[e^{\lambda_j t} \mu_j^{F'} + \mu_j^K \left(e^{\lambda_j t} - e^{\lambda_j (t-\tau)} \right) \right] \boldsymbol{\varphi}_j. \tag{3.50}$$

Since the $\boldsymbol{\varphi}_j$ build a basis of common eigenfunctions, they are linearly independent and one can compare coefficients in the above equation. This results in the following **characteristic equation for non–scalar TDF**:

$$\boxed{\lambda_j = \mu_j^{F'} + \mu_j^K (1 - e^{-\lambda_j \tau})} \tag{3.51}$$

Compared to the characteristic equation for scalar TDF (3.15), it looks like α was replaced by the eigenvalues of μ_j^K of $\underline{\underline{K}}$, although it is the other way round and all eigenvalues μ_j^K are equal to α, when considering the special case of scalar matrices:

$$\mu_j^K = \alpha \quad \forall j, \quad \text{if } \underline{\underline{K}} = \alpha \cdot \underline{\underline{1}}.$$

The same results as for the scalar TDF apply, when replacing $\alpha \to \mu_j^K$. If the eigenvalues μ_j^K can be freely chosen, this allows an individual control of the eigenmode $\boldsymbol{\varphi}_j$.

4 The Swift–Hohenberg Equation with Time Delayed Feedback Control

4.1 Introduction

In this chapter, we illustrate how the results obtained for general systems in chapter 3 can be applied for the Swift–Hohenberg equation (SHE) with time delayed feedback (TDF). We characterize the influence of TDF on the stability of patterns in a SHE in two dimensions and investigate which types of patterns emerge.

Since the Swift–Hohenberg equation without TDF is a gradient–system, all eigenvalues of the corresponding linear stability problem μ are real–valued. It was shown in chapter 3 that for $\mu \in \mathbb{R}$ system states can be destabilized by TDF, but not stabilized, therefore we focus on possible destabilization scenarios.

We extend the Swift–Hohenberg equation by introducing the TDF control term as an additional contribution, and obtain the Swift–Hohenberg equation with TDF, which also is denoted as the *Delayed Swift-Hohenberg equation* (DSHE) [TVT+10]:

$$\begin{aligned}\partial_t \psi(\boldsymbol{r},t) = \left[\epsilon - \left(k_c^2 + \nabla^2\right)^2\right] \psi(\boldsymbol{r},t) + \delta \cdot \psi(\boldsymbol{r},t)^2 - \psi^3(\boldsymbol{r},t) \\ + \alpha \left[\psi(\boldsymbol{r},t) - \psi(\boldsymbol{r},t-\tau)\right], \qquad (4.1)\end{aligned}$$

where α denotes the delay strength and τ denotes the delay time. For delay differential equations, the initial condition $g(\boldsymbol{r},t)$ has to be specified on the interval $[-\tau, 0]$:

$$\psi(\boldsymbol{r},t) = g(\boldsymbol{r},t), \quad t \in [-\tau, 0]. \qquad (4.2)$$

The DSHE transforms back into the SHE in the limit of vanishing control, i.e., for $\alpha \to 0$ or $\tau \to 0$, whereas for $\alpha \neq 0$ the gradient structure property is lost due to TDF. This allows complex eigenvalues and non–monotonous system dynamics, and gives rise to interesting spatio–temporal behaviour.

As discussed in chapter 3, in the presence of TDF, the set of steady state solutions persist, but their stability may change. We therefore consider stability properties of the homogeneous steady state, stripes and hexagons in the DSHE, after giving an introduction to its numerical treatment.

4.2 Numerical Treatment

The direct numerical simulations (DNS) of the DSHE can be carried out with the same technique as used for the Swift–Hohenberg equation (see section 2.5). In summary, we used a pseudo–spectral method in space and a semi–implicit Euler time stepping.

The linear part remains the same as for the SHE without TDF, whereas the contribution of the TDF control term is supplemented to the non-linear term:

$$\begin{aligned}\partial_t\psi(\boldsymbol{r},t) &= \underbrace{\left[\epsilon-(k_c^2+\Delta)^2\right]}_{L(\Delta)}\psi(\boldsymbol{r},t)+\underbrace{\delta\cdot\psi(\boldsymbol{r},t)^2-\psi^3(\boldsymbol{r},t)+\alpha\left[\psi(\boldsymbol{r},t)-\psi(\boldsymbol{r},t-\tau)\right]}_{N[\psi]} \\ &= L(\Delta)\quad\psi(\boldsymbol{r},t)+\quad N[\psi].\end{aligned}$$

With this modified non-linear part $N[\psi]$ which now includes the contribution of the TDF control, the same numerical scheme can be applied, as explained in section 2.5.

4.3 Homogeneous Steady State

For the Swift–Hohenberg equation without TDF, the linear stability analysis for the homogeneous steady state $\psi^{(0)}(\boldsymbol{r})=0$ was performed in section 2.3.1. We obtained the eigenvalue μ of the uncontrolled system state

$$\mu(\epsilon,k)=\epsilon-(k_c^2-k^2)^2, \tag{4.3}$$

when considering eigenfunctions $e^{i\boldsymbol{kr}}$, beeing plane waves. The critical wave number was rescaled to $k_c=1$. Since the eigenvalue $\mu(\epsilon,k)$ depends on the parameter ϵ and on the wave number k, the eigenvalue λ of the corresponding linear stability problem in the DSHE also depends on these parameters and Eq. (3.17) becomes

$$\lambda\left(n,\mu(\epsilon,k),\alpha,\tau\right)=\mu(\epsilon,k)+\alpha+\frac{1}{\tau}W_n\left(-\alpha\tau e^{-(\mu(\epsilon,k)+\alpha)\tau}\right),\quad n\in\mathbb{Z}, \tag{4.4}$$

To illustrate the dependence of λ on these parameters, we consider a stable homogeneous state

$$\epsilon=-1\rightarrow\mu(\epsilon,k)<0.$$

and try to destabilize it by the application of TDF with control parameters α and τ. Since $\mu(-1,k)<0\,\forall k$, the delay strength α must be chosen with positive sign, in order to be able to achieve a destabilization (see solvability condition in section 3.4.2). To get a first insight, it is instructive to map a reasonable choice of sets $\{n, k, \alpha, \tau\} \to \lambda(n, \mu(\epsilon = -1, k), \alpha, \tau)$, in order to get an overview of the spectrum $\{\lambda\}$, depicted in Fig. 4.1. Thereby, we can identify the branches n with the largest growth rate Re λ as $n = 0$ and $n = -1$, and furthermore shall see that they are the first branches which cross the imaginary axis and thus destabilize the homogeneous steady state. As expected from Eq. (3.29), all branches n have a non–vanishing oscillation frequency $\omega :=$ Im $\lambda \neq 0$, when crossing the imaginary axis.

To classify the physical behaviour, our goal is to identify the fastest growing wave number k_{max}, since it will determine the length scale of the occurring pattern, and the branches n which cross the imaginary axis and thereby destabilize the homogeneous steady state. Since the parameter space is high dimensional, this can only be made successively.

4.3.1 The First Unstable Branch

First, we investigate which branch is the first branch that becomes unstable, when varying TDF control parameters (α, τ). To this end, we consider the growth rate

$$\max_k \text{Re } \lambda(n, \mu(\epsilon, k), \alpha, \tau) \quad \text{vs.} \quad (\alpha, \tau)$$

for fixed ϵ and at the wave number k_{max} which maximimizes it (see Fig. 4.2). Figure 4.2 shows that the first unstable branches are $n = 0$ and $n = -1$, which we denote as the *leading branches* as they govern the primary destabilization of $\psi^{(0)}$.

Since Fig. 4.2 shows only values with Re $\lambda \geq 0$, the boundary of these regions satisfy Re $\lambda = 0$ and are given by the obtained neutral stability curves for $\mu \in \mathbb{R}$ from Eq. (3.40), provided that their construction was appropriate and their indices m match the branch indices n of our solution in terms of the Lambert–W function. To provide a proof of concept, Fig. 4.3 shows the leading branches $n = 0$ and $n = -1$ and the corresponding neutral stability curve $\tau_c(m, \mu, \alpha)$ with index $m = 0$, which shows good agreement.

4.3.2 Fastest Growing Wave Number k_{max} and Bifurcation Type

The classical method to determine the fastest wave number k_{max} and the type of bifurcation, being of monotonic or oscillatory nature, is to consider Re λ and Im λ vs. k (see Fig. 4.4), from which this information is clear from inspection. From Fig. 4.4, we can conclude the existence of a traveling wave bifurcation with wave number k_{max} and its special case, the homogenous Hopf background oscillation at

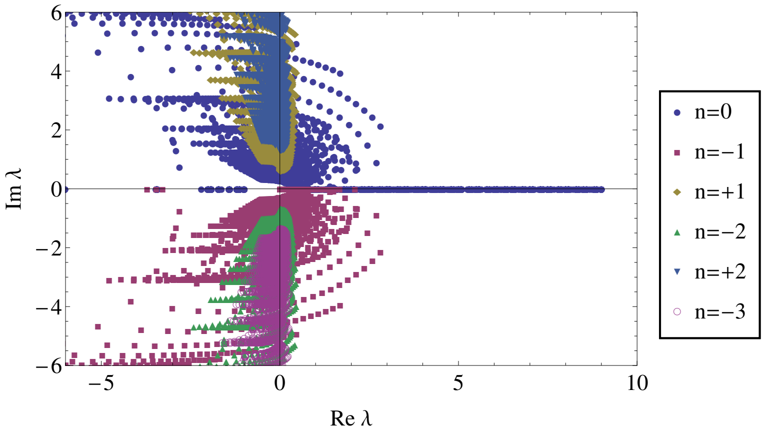

(a)

↓ zoom for Re $\lambda > 0$

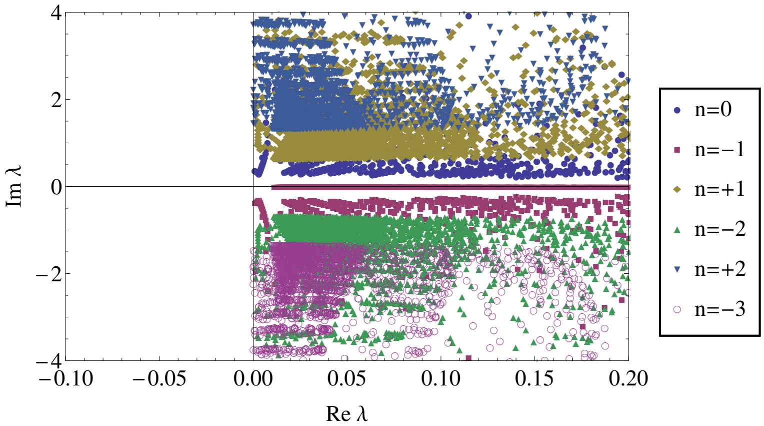

(b)

Figure 4.1: Spectrum $\lambda(n, \mu(-1, k), \alpha, \tau)$ for a set of $\{n, k, \alpha, \tau\}$. Parameter ranges are $k \in [0, 3]$, $\alpha \in [0, 10]$, $\tau \in [0, 10]$ for branches $-3 \leq n \leq 2$. Since the spectrum continously depends on the control parameters, it would cover the whole area if visualized for continous parameters. Therefore, the chosen paramater ranges are discretized as $\Delta k = 0.3$, $\Delta\alpha = 0.5$ and $\Delta\tau = 0.5$. Branches appear in the legend in order of grouping of near–conjugate branch pairs. a) It can be observed that the branches n build near–conjugate branch pairs, as expected from the Lambert–W function. Branches with largest growth rate Re λ are $n = 0$ and $n = -1$. b) When eigenvalues λ cross the imaginary axis due to destabilization of $\mu \in \mathbb{R}_-$, their corresponding oscillation frequency $\omega :=$ Im $\lambda \neq 0$ is non–zero, as expected from Eq. (3.29).

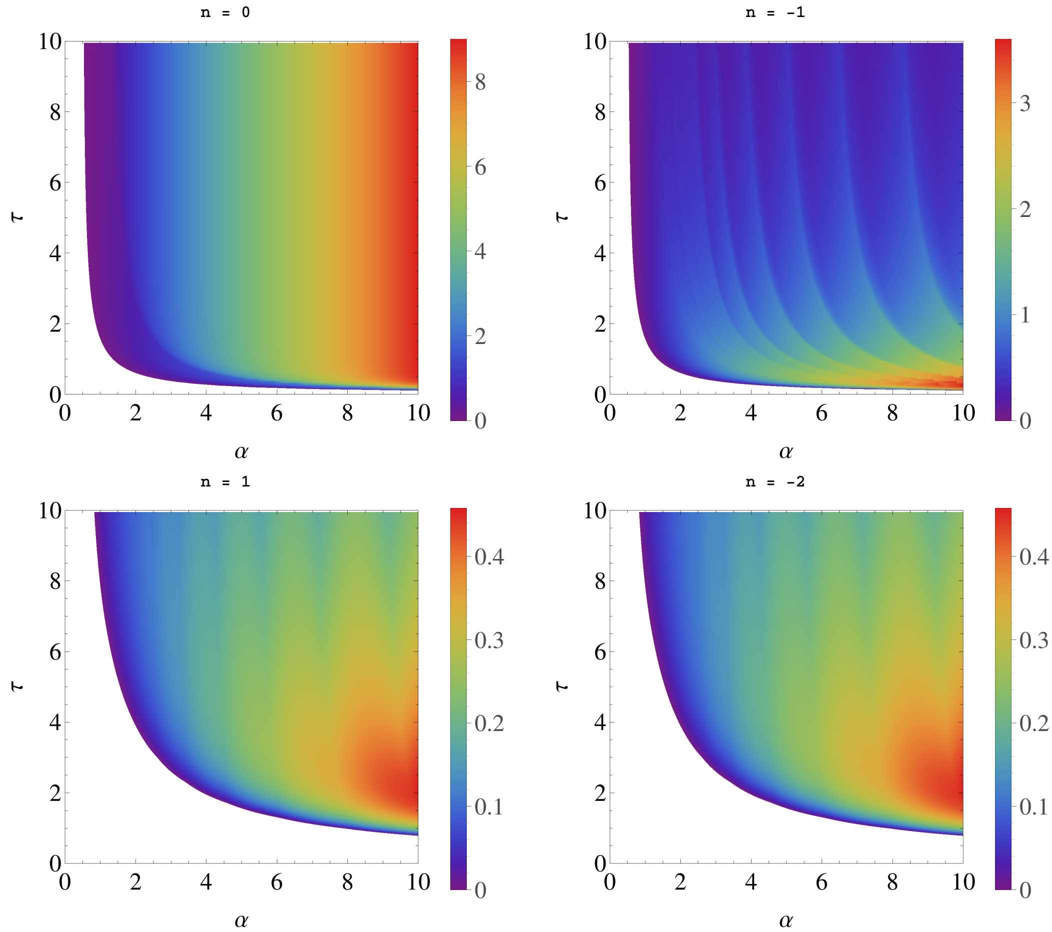

Figure 4.2: Re $\lambda(n, \mu(\epsilon, k_{max}), \alpha, \tau)$ vs. (α, τ) for fixed $\epsilon = -1$ and at fastest growing wave number k_{max}, which was found by numerical maximization with respect to k. Only values with Re $\lambda \geq 0$ are shown. It can be observed, that the branches $n = 0$ and $n = -1$ are the first branches that become unstable (see top panel), when varying α and τ, whereas $n = 1$, $n = -2$ become unstable for larger α and τ (see bottom panel).

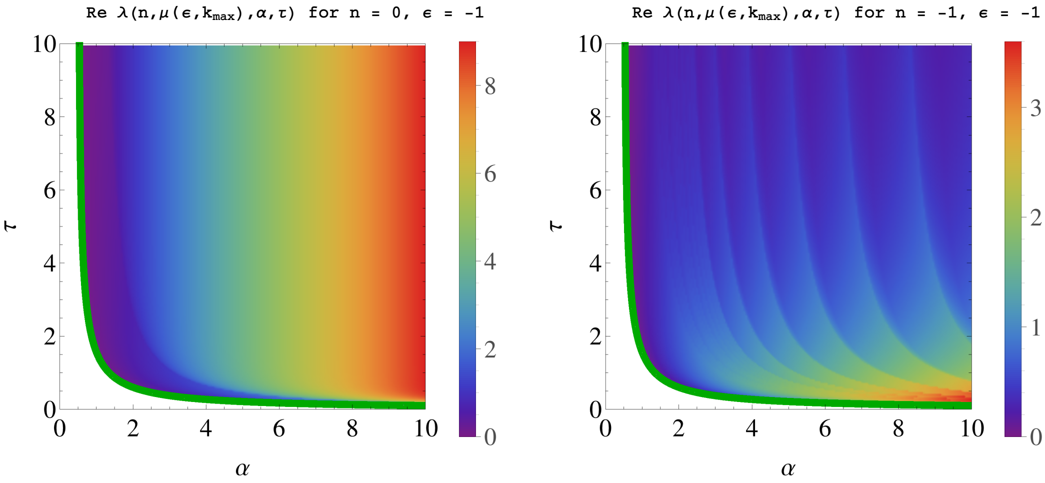

Figure 4.3: Leading branches $n = 0$, $n = -1$ with neutral stability curve. Since only values with Re $\lambda \geq 0$ are shown, the boundary of these regions satisfy Re $\lambda = 0$. By construction, the curve which describes the boundary shall be the neutral stability curve for $\mu \in \mathbb{R}$ as obtained from Eq. 3.40. The neutral stability curve $\tau_c(m, \mu, \alpha)$ for $m = 0$, represented by the green line, shows good agreement with this boundary and therefore indeed describes the change of stability.

$k = 0$ for a selection of α and τ.

Since the parameter space is high-dimensional, this approach can only be performed for particular choices of α and τ, and therefore does not provide information for all α and τ at once. It was observed in Fig. 4.4 that the fastest growing wave number k_{max} could depend on α and τ and on the particular branch n. Therefore, it is instructive to consider a global method to find $k_{max}(n, \alpha, \tau)$; similar to the consideration of the spectrum $\{\lambda\}$ in Fig. 4.1, which revealed that all unstable branches have a non–vanishing oscillation frequency Im λ when crossing the imaginary axis.
To this end, Fig. 4.5 shows an extension of Fig. 4.2 to the third dimension, specifying k_{max}. It can be seen that the overall fastest growing wave number is $k_{max} = k_c = 1$ for branch $n = 0$. Presumably the fastest growing wave numbers $k_{max} \neq 1$ of other branches are not relevant, since the destabilization is dominated by $k_{max} = 1$ for branch $n = 0$, which has the overall largest growth rate Re λ of all branches.

Combining the global information about the spectrum from Fig. 4.1 and the fastest growing wave number k_{max} from Fig. 4.5, it can be stated that the *destabilization of the homogeneous steady state* $\psi^{(0)}(\boldsymbol{r}) = 0$ occurs via a *traveling wave bifurcation*, since predominantly the fastest growing wave number is $k_{max} = 1$ and its corresponding oscilation frequeny Im λ is non–zero. Figure 4.6 compares our analytical prediction to a direct numerical simulation of the discussed destabilization scenario for $\mu(-1, k)$, which shows good agreement.

4.4 Stripes and Hexagons

The linear stability analysis of stripes and hexagons in the DSHE is analogous to the performed analysis for the SHE without TDF, as presented in section 2.3.2. In summary, we make a general ansatz, which incorporates both stripes and hexagons as a special case; derive the amplitude equations for the complex amplitude $\xi_j \in \mathbb{C}$ by the mode projection technique; split the amplitude equations into the real amplitudes R_j and phases φ; and then consider the linear stability problem for the special case of stripes or hexagons. The following analysis therefore focuses on the relevant details. In Fig. 2.4, we illustrated the motivation for making the following ansatz:

$$\psi(\boldsymbol{r}, t) = \sum_{j=1}^{3} \xi_j e^{i\boldsymbol{k_j r}} + c.c. \tag{4.5}$$

$$= \sum_{j=1}^{3} |\xi_j| \cos(\boldsymbol{k}_j \boldsymbol{r} + \varphi_j), \tag{4.6}$$

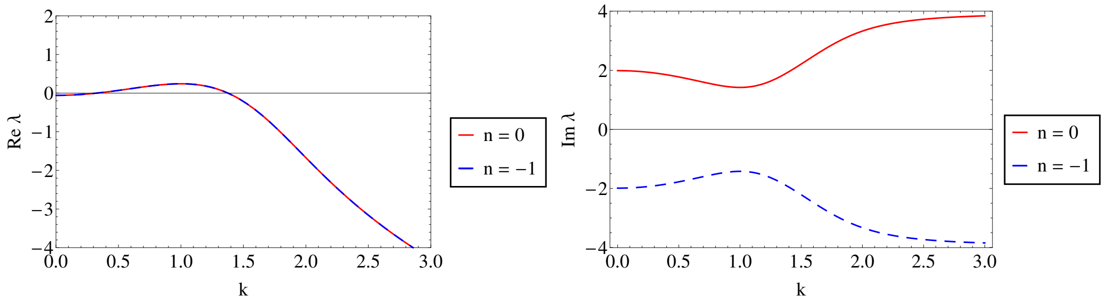

(a)

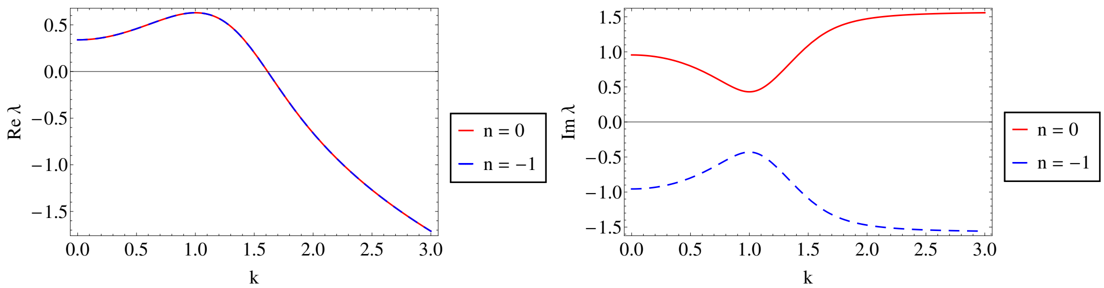

(b)

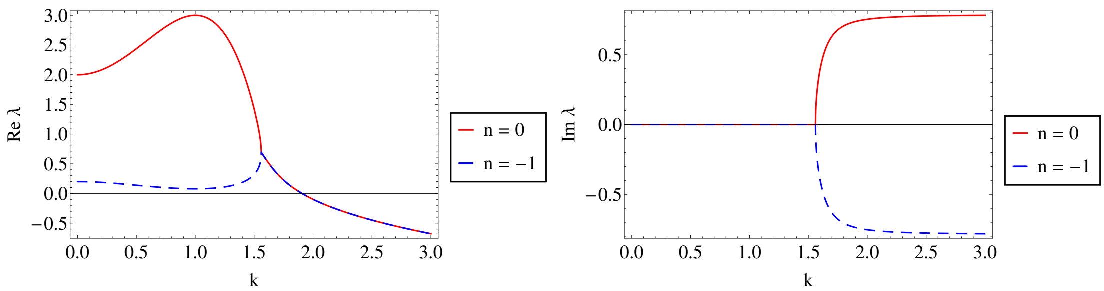

(c)

Figure 4.4: Real (left) and imaginary (right) parts of $\lambda(n, \mu(-1, k), \alpha, \tau)$ vs. k for the leading branches $n = 0$, $n = -1$. The bifurcation type is clear from inspection: a) $\alpha = 1.9$, $\tau = 0.8$: Traveling wave bifurcation with $k_{max} = 1$. b) $\alpha = 2$, $\tau = 2$: Traveling wave bifurcation at $k_{max} = 1$ with Hopf background oscillations with $k = 0$. c) $\alpha = 4$, $\tau = 4$: Traveling wave bifurcation at $k_{max} = 1$ for branch $n = 0$, traveling wave bifurcation at $k_{max} \approx 1.6$. A homogeneous Hopf oscillation arises for both branches. The merging of branches $n = 0$ and $n = -1$ is a result of crossing the branch point of the Lambert–W function; the merging arises before the transition through zero in Re $\lambda(k)$.

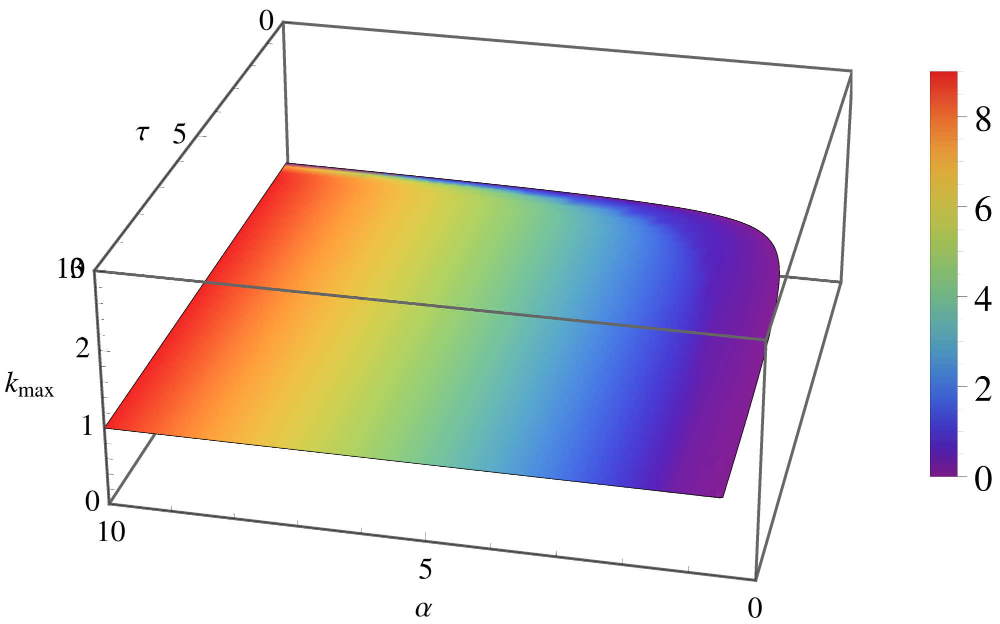

(a) $n = 0$

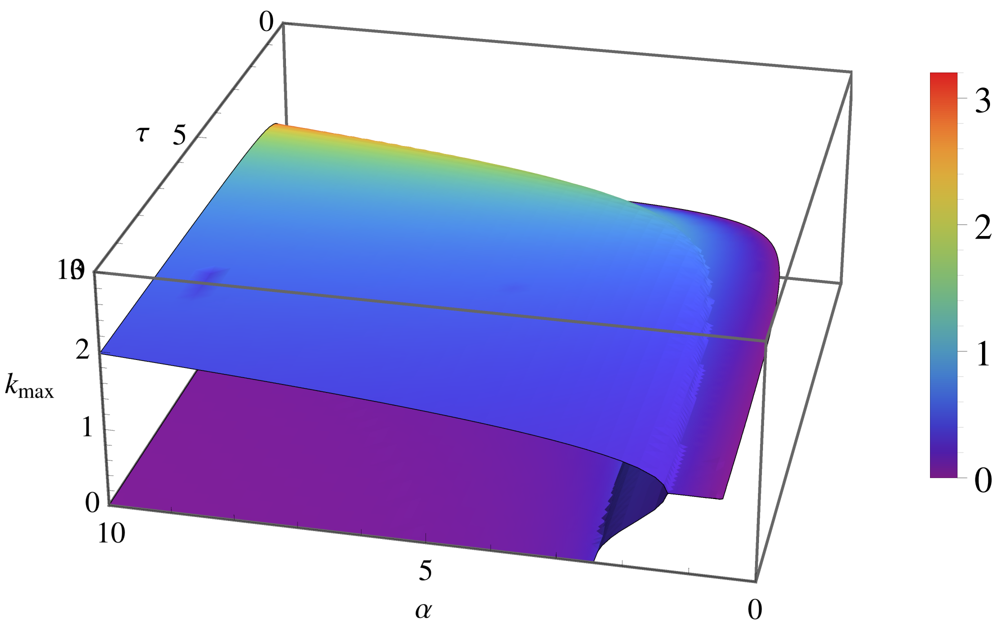

(b) $n = -1$

Figure 4.5: $k_{max}(n, \alpha, \tau)$ vs. (α, τ) for $\epsilon = -1$. This is an extension of Fig. 4.2 to the third dimension, specifying the local maxima of Re λ with respect to k. The viewpoint is chosen such that the splitting of k_{max} can be observed. Colours specify the values of Re $\lambda(n, \mu(\epsilon, k_{max}), \alpha, \tau)$. a) For the branch $n = 0$, the fastest growing wave number is $k_{max} = 1$ for all $(\alpha,\ \tau)$. b) For the branch $n = -1$, the fastest growing wave number is $k_{max} = 1$ at the bifurcation curve and depends on parameters $(\alpha,\ \tau)$ further away from the bifurcation.

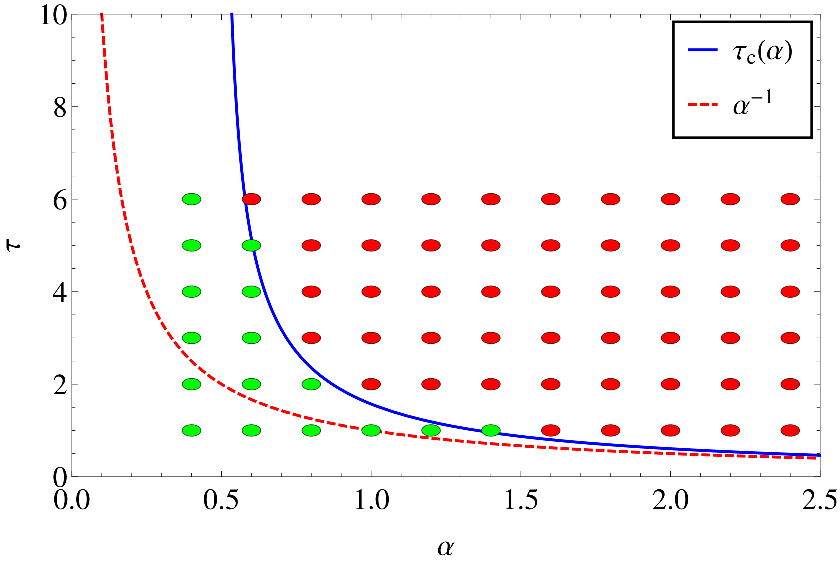

Figure 4.6: Comparison of analytical predictions with a direct numerical simulation of a destabilization scenario of the *homogeneous steady state* for fixed $\epsilon = -1$. Green (red) points indicate that the homogeneous steady state is stable (unstable), when subjected to TDF with delay strength α and delay time τ. The change of stability is well described by the obtained neutral stability curve $\tau_c(\alpha)$ from Eq. (3.40). The red dotted curve was obtained from the consideration of the limit of small delay times τ in section 3.2, and it can be observed that the neutral stability curve converges to it. Simulation parameters are: $\epsilon = -1$, $\delta = 0$, initial cond.$= 0 +$ noise, TDF turned on at time $T = 0$.

with complex amplitudes $\xi_j(t) \in \mathbb{C}$ and wave vectors $\boldsymbol{k}_j$:

$$\boldsymbol{k}_1 = k_c \begin{pmatrix} 1 \\ 0 \end{pmatrix}, \quad \boldsymbol{k}_2 = \frac{k_c}{2} \begin{pmatrix} -1 \\ \sqrt{3} \end{pmatrix}, \quad \boldsymbol{k}_3 = \frac{k_c}{2} \begin{pmatrix} -1 \\ -\sqrt{3} \end{pmatrix}. \tag{4.7}$$

As stated earlier, this ansatz contains both stripes and hexagons. One obtains hexagons by considering

$$|\xi_1| = |\xi_2| = |\xi_3| \tag{4.8}$$

and stripes by setting

$$|\xi_1| \neq 0, \quad |\xi_2| = |\xi_3| = 0. \tag{4.9}$$

The non–zero amplitude $|\xi_j| \neq 0$ can be arbitrarily chosen.

When substituting the ansatz (4.5) in the Swift–Hohenberg equation with TDF (4.1) and projecting on the modes $e^{i\boldsymbol{k}_j\boldsymbol{r}}$ of the ansatz, one obtains the amplitude equations for the complex amplitudes $\xi_j \in \mathbb{C}$ in the presence of TDF. They read:

$$\dot{\xi}_1 = \epsilon\xi_1 + 2\delta\xi_2^*\xi_3^* - 3\xi_1 \left[|\xi_1|^2 + 2|\xi_2|^2 + 2|\xi_3|^2\right] + \alpha\left(\xi_1(t) - \xi_1(t-\tau)\right), \tag{4.10a}$$

$$\dot{\xi}_2 = \epsilon\xi_2 + 2\delta\xi_3^*\xi_1^* - 3\xi_2 \left[2|\xi_1|^2 + |\xi_2|^2 + 2|\xi_3|^2\right] + \alpha\left(\xi_2(t) - \xi_2(t-\tau)\right), \tag{4.10b}$$

$$\dot{\xi}_3 = \epsilon\xi_3 + 2\delta\xi_1^*\xi_2^* - 3\xi_3 \left[2|\xi_1|^2 + 2|\xi_2|^2 + |\xi_3|^2\right] + \alpha\left(\xi_3(t) - \xi_3(t-\tau)\right). \tag{4.10c}$$

One can observe that these are our earlier obtained amplitude equations from Eq. (2.17) being extended by TDF control terms. The TDF control terms add linearly to the amplitude equations, since the control mechanism is linear and additive, and the ansatz consist of a linear superposition of plane waves.

If, at this point, we would consider stripes in Eq. (4.10), this would result in the same amplitude equation as found in [ITSO13], beeing derived for stripes in the the Lengyel–Epstein model with TDF. Pursueing our more general ansatz, we split the complex amplitudes $\xi_j(t) = R_j(t)e^{i\varphi_j(t)}$ in Eq. (4.10) into their real amplitudes

$R_j(t)$ and phases $\varphi_j(t)$, which yields:

$$\begin{aligned}
\dot{R}_1 &= \epsilon R_1 + 2\delta \cdot R_2 R_3 \cos(\varphi_1 + \varphi_2 + \varphi_3) - 3R_1 \left[R_1^2 + 2R_2^2 + 2R_3^2\right] \\
&\quad + \alpha \left[R_1(t) - R_1(t-\tau)\cos(\varphi_1(t) - \varphi_1(t-\tau))\right], && (4.11a)\\
\dot{R}_2 &= \epsilon R_2 + 2\delta \cdot R_3 R_1 \cos(\varphi_1 + \varphi_2 + \varphi_3) - 3R_2 \left[2R_1^2 + R_2^2 + 2R_3^2\right] \\
&\quad + \alpha \left[(R_2(t) - R_2(t-\tau)\cos(\varphi_2(t) - \varphi_2(t-\tau))\right], && (4.11b)\\
\dot{R}_3 &= \epsilon R_3 + 2\delta \cdot R_1 R_2 \cos(\varphi_1 + \varphi_2 + \varphi_3) - 3R_3 \left[2R_1^2 + 2R_2^2 + R_3^2\right] \\
&\quad + \alpha \left[R_3(t) - R_3(t-\tau)\cos(\varphi_3(t) - \varphi_3(t-\tau))\right], && (4.11c)\\
R_1\dot{\varphi}_1 &= -2\delta \cdot R_2 R_3 \sin(\varphi_1 + \varphi_2 + \varphi_3) + \alpha R_1(t-\tau)\sin(\varphi_1(t) - \varphi_1(t-\tau)), && (4.11d)\\
R_2\dot{\varphi}_2 &= -2\delta \cdot R_3 R_1 \sin(\varphi_1 + \varphi_2 + \varphi_3) + \alpha R_2(t-\tau)\sin(\varphi_2(t) - \varphi_2(t-\tau)), && (4.11e)\\
R_3\dot{\varphi}_3 &= -2\delta \cdot R_1 R_2 \sin(\varphi_1 + \varphi_2 + \varphi_3) + \alpha R_3(t-\tau)\sin(\varphi_3(t) - \varphi_3(t-\tau)), && (4.11f)
\end{aligned}$$

Since the TDF term vanishes at the steady states, the stripe and the hexagon steady state solution persist, but their stability may change due to TDF. The linear stability analysis for both solutions is straightforward and allows to clarify the stability properties of stripes and hexagons in the Swift–Hohenberg equation with TDF.

4.4.1 Linear Stability of Stripes

First, we consider the corresponding linear stability problem for stripes. For the small perturbations $\delta R_j(t)$ of the real stationary amplitudes $R_j^{(0)} = \left(\frac{\sqrt{\epsilon}}{3}, 0, 0\right)^T$ (see Eq. (2.26)), one obtains

$$\frac{d}{dt}\begin{pmatrix}\delta R_1(t)\\ \delta R_2(t)\\ \delta R_3(t)\end{pmatrix} = \underbrace{\begin{pmatrix}-2\epsilon & 0 & 0\\ 0 & -\epsilon & 2\delta \cdot R_1^{(0)}\\ 0 & 2\delta \cdot R_1^{(0)} & -\epsilon\end{pmatrix}}_{=:\underline{\underline{S}}^R} \cdot \begin{pmatrix}\delta R_1(t)\\ \delta R_2(t)\\ \delta R_3(t)\end{pmatrix} + \alpha \cdot \underline{\underline{1}} \begin{pmatrix}\delta R_1(t) - \delta R_1(t-\tau)\\ \delta R_2(t) - \delta R_2(t-\tau)\\ \delta R_3(t) - \delta R_3(t-\tau)\end{pmatrix}.$$

The matrix $\underline{\underline{S}}^R$ is the same as in the linear stability problem of amplitude perturbations δR_j without TDF which we obtained in Eq. (2.29), and we already calculated its eigenvalues μ^R : $\mu_1^R = -2\epsilon$, $\mu_2 = -\epsilon - 2\delta \cdot R_1^{(0)}$ and $\mu_3^R = -\epsilon + 2\delta \cdot R_1^{(0)}$. The phase stability problem for the small perturbation $\delta\varphi_1(t)$ of the phase $\varphi_1^{(0)}$ yields:

$$\frac{d}{dt}\,\delta\varphi_1(t) = 0 \cdot \delta\varphi_1(t) + \alpha(\delta\varphi_1(t) - \delta\varphi_1(t-\tau)).$$

The eigenvalue of the linear stability problem for the phase perturbation is $\mu^{\varphi} = 0$. One can see that both equations are prototypes of TDF control with scalar coupling matrices $\underline{\underline{K}} = \alpha \cdot \underline{\underline{1}}$ and our analysis applies, since it was already shown that the matrix $\underline{\underline{S}}^R$ is diagonalizable.

Relating to the observations for the oscillation frequency $\omega := \mathrm{Im}\,\lambda$ at the onset of the bifurcation (see section 3.4.2), the following TDF–induced bifurcation scenarios can be identified:

- Since $\mu_j^R < 0\,\forall j$ holds for stable stripes, we know that the occurring instability is of oscillatory type and that the fastest growing wave number is $k = k_c$, since is was part of our ansatz with which we derived the amplitude equations. Therefore, a destabilization of an eigenvalue $\mu_j^R < 0$ via TDF results in a *traveling wave bifurcation*.
- As explained, a destabilization of the eigenvalue $\mu^\varphi = 0$ of the phase linear stability problem involves a *drift bifurcation at $\alpha\tau = 1$*, which is observed to be the first bifurcation for the DSHE.

Figure 4.7 compares our analytical prediction to a direct numerical simulation of a destabilization scenario of stripes, which shows good agreement.

4.4.2 Linear Stability of Hexagons

We consider the corresponding linear stability problem for hexagons. For the small perturbations $\delta R_j(t)$ to the real stationary amplitudes $R_j^{(0)} = R_h\,(1,1,1)^T$, $R_h = \frac{1}{15}\left((-1)^n\delta \pm \sqrt{\delta^2 + 15\epsilon}\right)$, one obtains

$$\frac{d}{dt}\begin{pmatrix}\delta R_1(t)\\ \delta R_2(t)\\ \delta R_3(t)\end{pmatrix} = \underbrace{\begin{pmatrix}A & B & B\\ B & A & B\\ B & B & A\end{pmatrix}}_{=:\underline{\underline{S}}^R} \cdot \begin{pmatrix}\delta R_1(t)\\ \delta R_2(t)\\ \delta R_3(t)\end{pmatrix} + \alpha \cdot \underline{\underline{1}} \begin{pmatrix}\delta R_1(t) - \delta R_1(t-\tau)\\ \delta R_2(t) - \delta R_2(t-\tau)\\ \delta R_3(t) - \delta R_3(t-\tau)\end{pmatrix}.$$

with the abbreviations $A = \epsilon - 21R_h^2$ and $B = 2\delta \cdot R_h - 12R_h^2$. For the small perturbations $\delta\varphi_j(t)$ to the phases $\varphi_j^{(0)}$, one obtains:

$$\frac{d}{dt}\begin{pmatrix}\delta\varphi_1(t)\\ \delta\varphi_2(t)\\ \delta\varphi_3(t)\end{pmatrix} = \underbrace{-2\delta \cdot R_h \begin{pmatrix}1 & 1 & 1\\ 1 & 1 & 1\\ 1 & 1 & 1\end{pmatrix}}_{=:\underline{\underline{S}}^\varphi} \cdot \begin{pmatrix}\delta\varphi_1(t)\\ \delta\varphi_2(t)\\ \delta\varphi_3(t)\end{pmatrix} + \alpha \cdot \underline{\underline{1}} \begin{pmatrix}\delta\varphi_1(t) - \delta\varphi_1(t-\tau)\\ \delta\varphi_2(t) - \delta\varphi_2(t-\tau)\\ \delta\varphi_3(t) - \delta\varphi_3(t-\tau)\end{pmatrix}.$$

Our analysis applies, for the same reasons as stated for stripes. It was already shown that the matrices $\underline{\underline{S}}^R$ and $\underline{\underline{S}}^\varphi$ can be diagonalized and one can calculate the eigenvalues μ_j^R and μ_j^φ, respectively. Again, one obtains a traveling wave bifurcation if

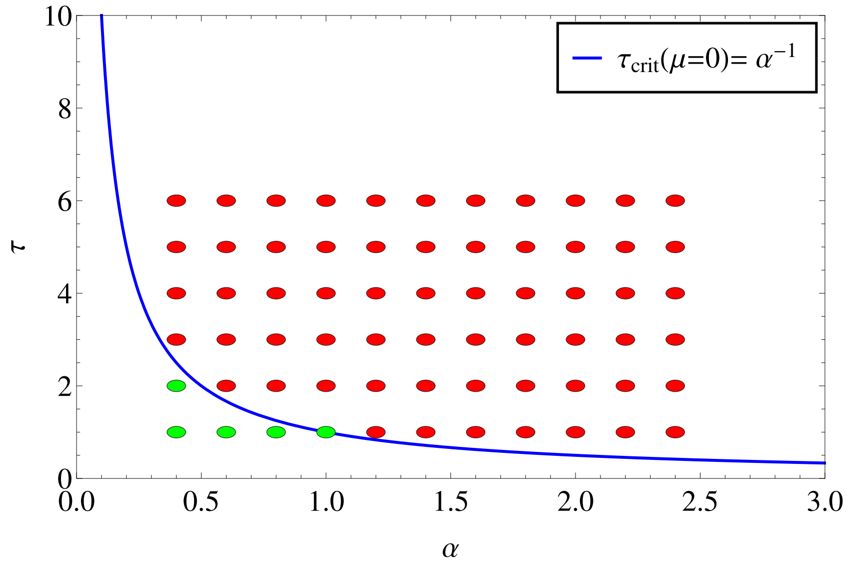

Figure 4.7: Comparison of analytical predictions with a direct numerical simulation of a destabilization scenario of *stripes*. Green (red) points indicate that the stripes steady state is stable (unstable), when subjected to TDF with delay strength α and delay time τ. The change of stability is well described by the obtained neutral stability curve $\tau_c(\alpha)$ from our analytical considerations. The first eigenvalue that becomes unstable is $\mu = 0$, which creates a drift bifurcation. Simulation parameters are: $\epsilon = 1$, $\delta = 0$, initial cond.$= 0 + noise$, TDF turned on at time $T = 500$ after the stripes have fully developed.

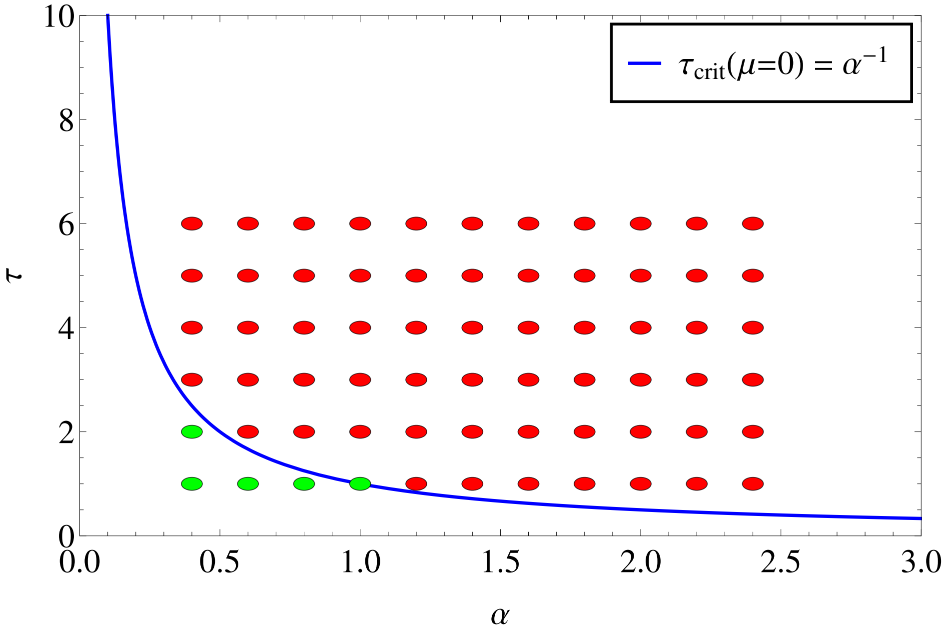

Figure 4.8: Comparison of analytical predictions with a direct numerical simulation of a destabilization scenario of *hexagons*. Green (red) points indicate that the hexagon steady state is stable (unstable), when subjected to TDF with delay strength α and delay time τ. The change of stability is well described by the obtained neutral stability curve $\tau_c(\alpha)$ from our analytical considerations. The first eigenvalue that becomes unstable is $\mu = 0$, which creates a drift bifurcation. Simulation parameters are: $\epsilon = 1$, $\delta = 1$, initial cond.$= 0 + \textit{noise}$, TDF turned on at time $T = 500$ after the hexagons have fully developed.

any of the $\mu_j^R < 0$ is destabilized via TDF, whereas a drift bifurcation sets in when $\mu^\varphi = 0$ is destabilized.

Figure 4.8 compares our analytical results with a numerical simulation of a destabilization scenario of hexagons, and confirms our theoretical predictions.

4.5 Common and Uncommon Arising Numerical Solutions

The homogeneous steady state $\psi^{(0)}(\boldsymbol{r}) = 0$ always loses stability in a traveling wave bifurcation, which then obviously can lead to a traveling wave pattern (see Fig. 4.9). However, for some TDF control parameter values (α, τ) further away from the bifurcation curve, numerical solutions were found in which an oscillation between two opposite states was observed for larger times (see Fig. 4.10).

The inhomogeneous solutions, namely stripes and hexagons, lose stability in a drift bifurcation at $\alpha\tau = 1$, when the phase eigenvalue $\mu^{\varphi} = 0$ is destabilized via TDF; followed by a traveling wave bifurcation, when the amplitude eigenvalue $\mu^{R} < 0$ is destabilized. Numerical solutions for TDF control parameter values which cause a traveling wave bifurcation are qualitatively the same as shown in Fig. 4.9.

However, the most interesting scenarios are those where TDF control parameters lie in–between the drift and the traveling wave bifurcation curve, i.e., where an eigenmode with eigenvalue $\mu = 0$ is destabilized, but eigenmodes with eigenvalues $\mu < 0$ are not. For instance, we observed a drift bifurcation of hexagons (see Fig. 4.11), but also unexpected numerical solutions for stripes, such as the following:

- Starting with stripes with wave number $k = k_c$, we observed a ZigZag instability of stripes which then started to drift (see Fig. 4.12), although the parameter setting is not ZigZag–unstable in the Swift–Hohenberg equation without TDF.
- Starting with stripes with $k > k_c$ which would result in an Eckhaus instability in the Swift–Hohenberg equation without TDF, we observed a drift bifurcation of these stripes (see Fig. 4.13), when subjected to TDF.

Therefore, according to numerical observations, it can be concluded that the Eckhaus and ZigZag instability, or in general the Benjamin–Feir instability, is influenced by TDF and their regions of instability became larger in parameter space.

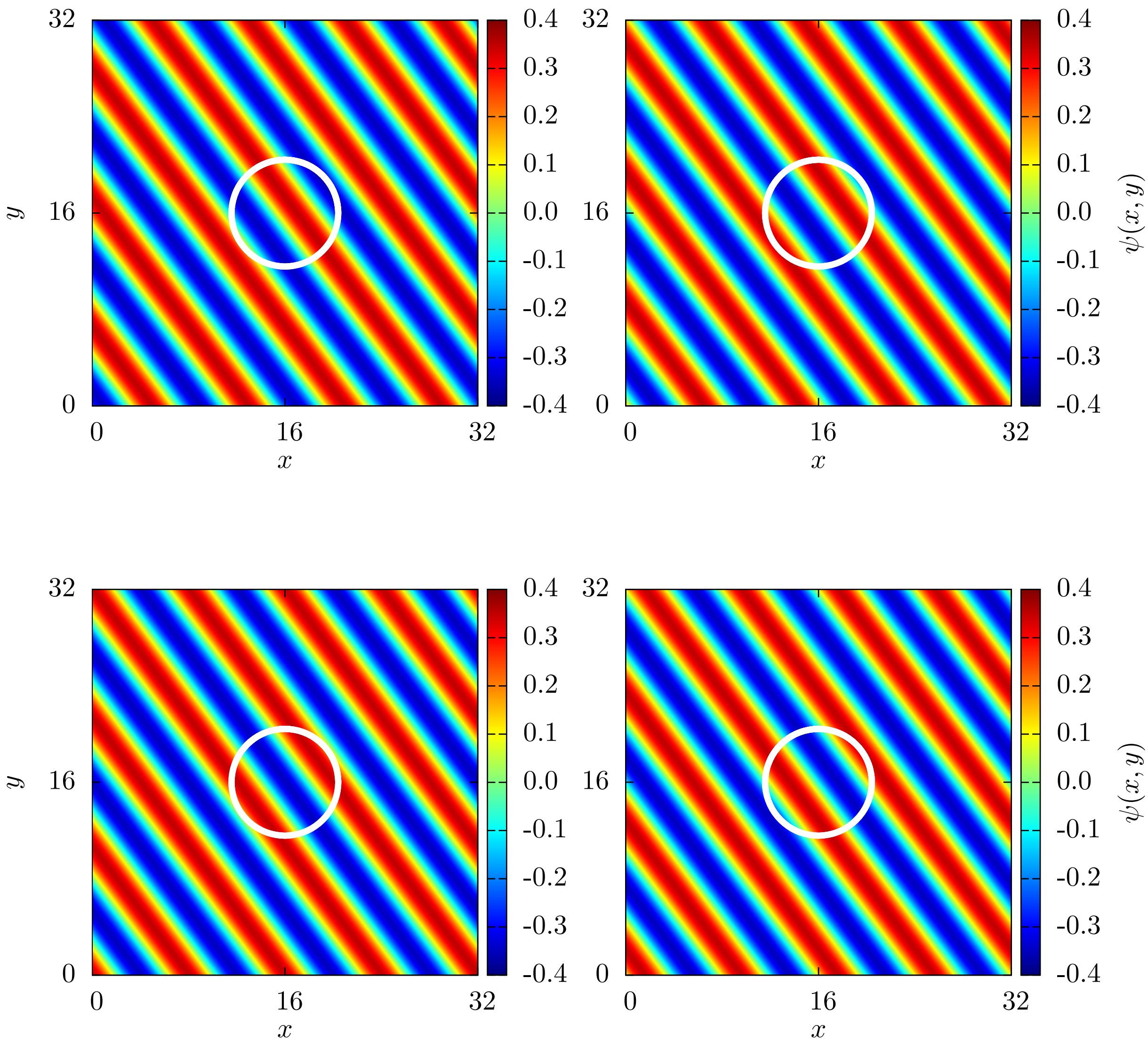

Figure 4.9: Snapshot of a traveling wave solution, as a result of destabilizing the homogeneous steady state by TDF. The white circle is a reference point and shows that the traveling wave moves towards the top right corner. Paramaters are: $\epsilon = -1$, $\delta = 0$, $\alpha = 1.9$, $\tau = 0.8$, start with $0 + noise$, TDF turned on at $T = 0$.

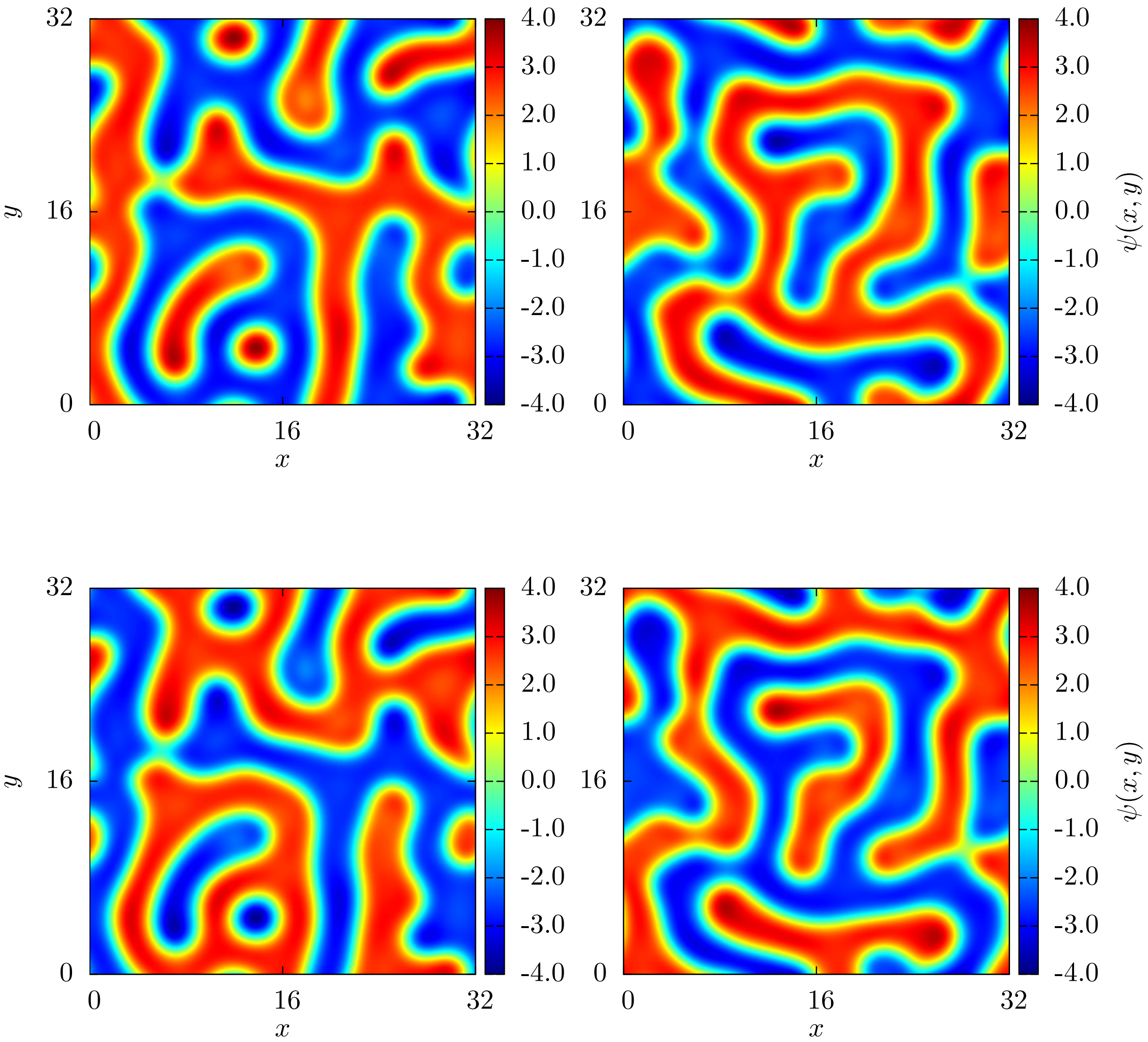

Figure 4.10: Snapshots of an oscillation between two opposite states, as a result of destabilizing the homogeneous steady state by TDF. Parameters are: $\epsilon = -1$, $\delta = 0$, $\alpha = 4$, $\tau = 4$, start with $0 + noise$, TDF turned on at $T = 0$

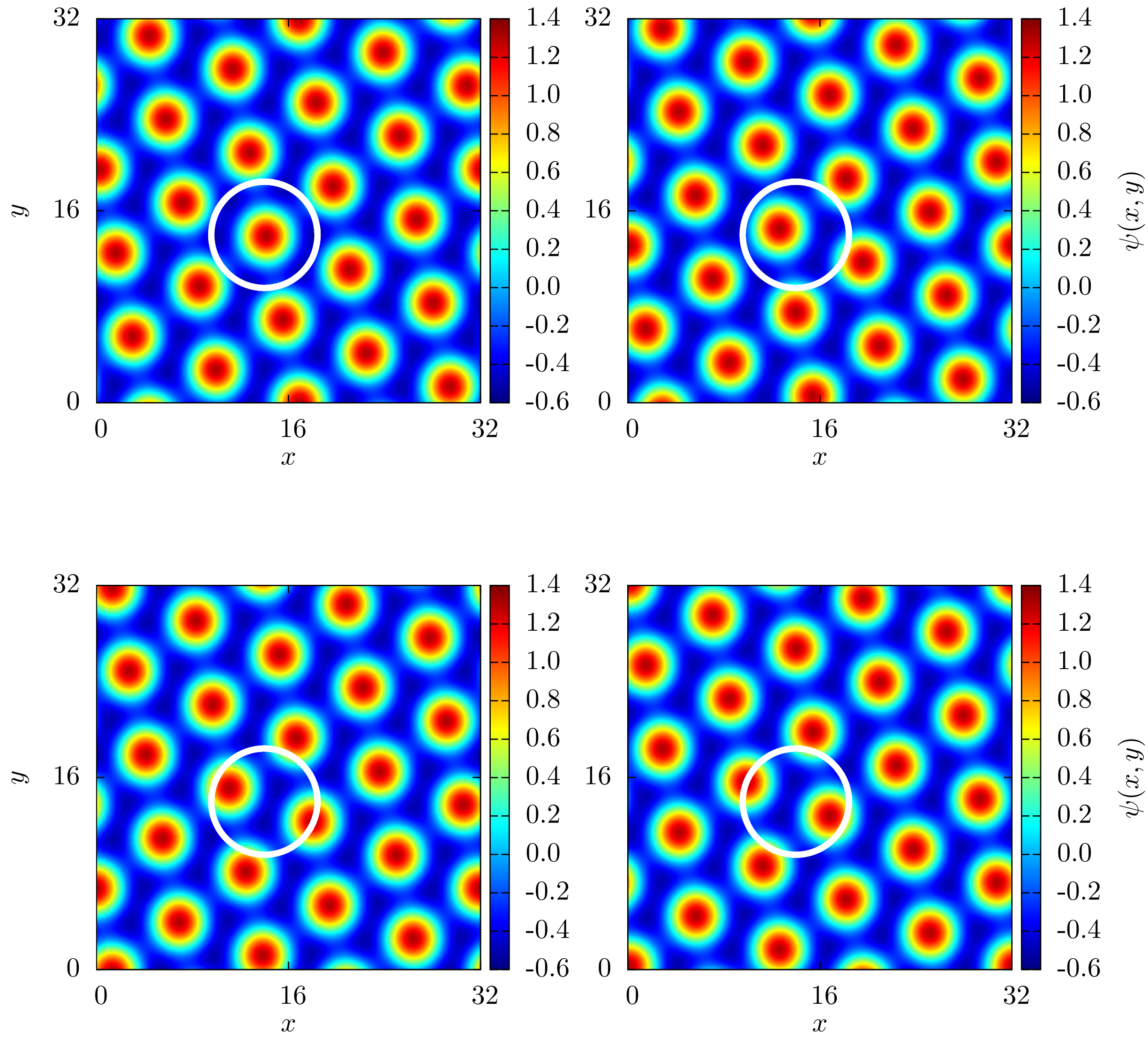

Figure 4.11: Snapshot of a drift bifurcation of hexagons. The white circle is a reference point, which allows to identify the movement to the left top. Parameters are: $\epsilon = 0.1$, $\delta = 1.0$, $\alpha = 0.5$, $\tau = 2.2$, start with $0 + noise$, TDF turned on after hexagons relaxed in their steady state.

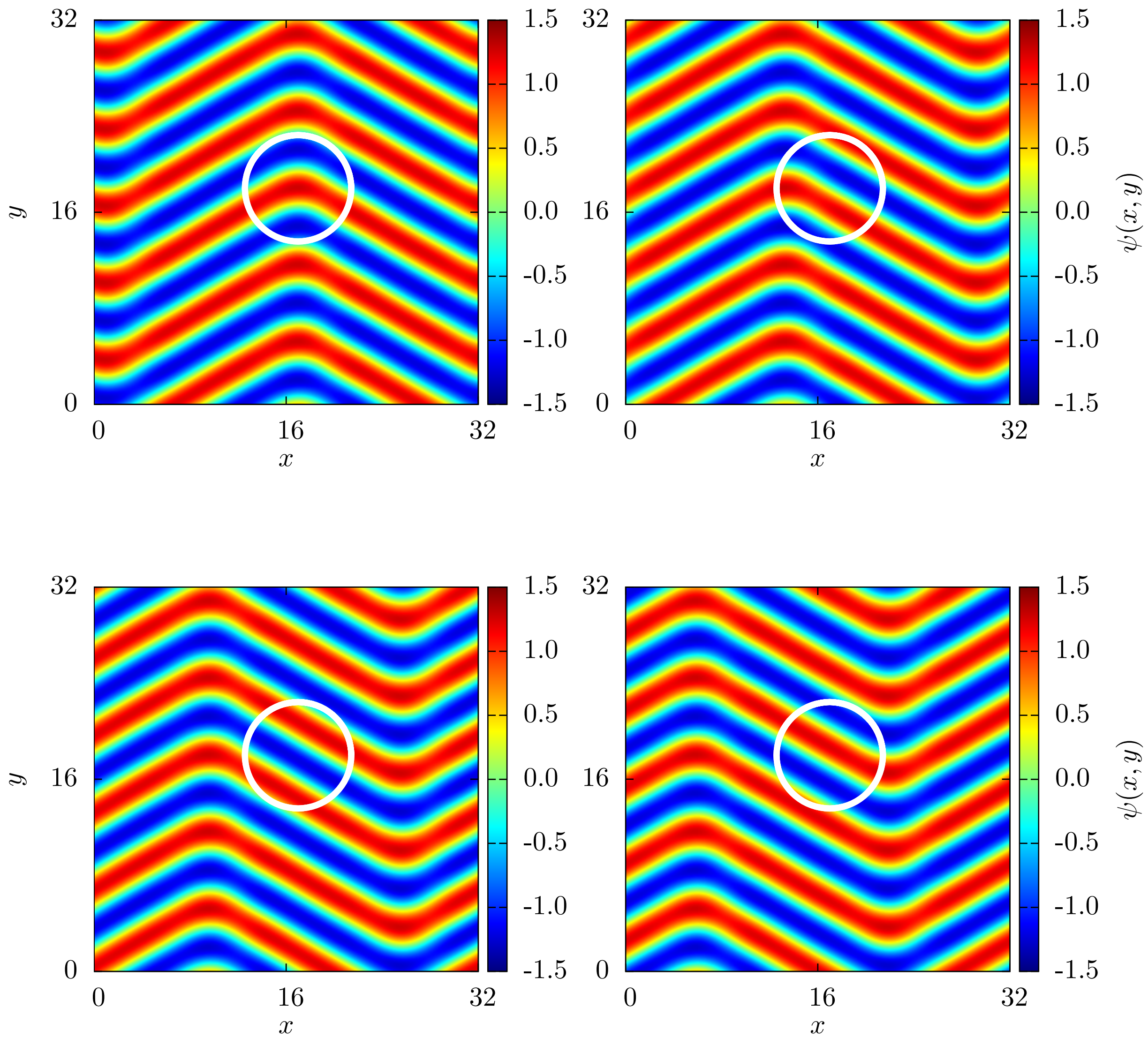

Figure 4.12: Snapshot of a drift bifurcation of a ZigZag pattern. The white circle is a reference point, which allows to identify the movement to the left. Parameters are: $\epsilon = 1$, $\delta = 0$, $\alpha = 0.5$, $\tau = 2.2$, start with $\sin(k_c y)$, where $k_c = 1$ is the critical wave number. TDF was turned on after the relaxation into stripes.

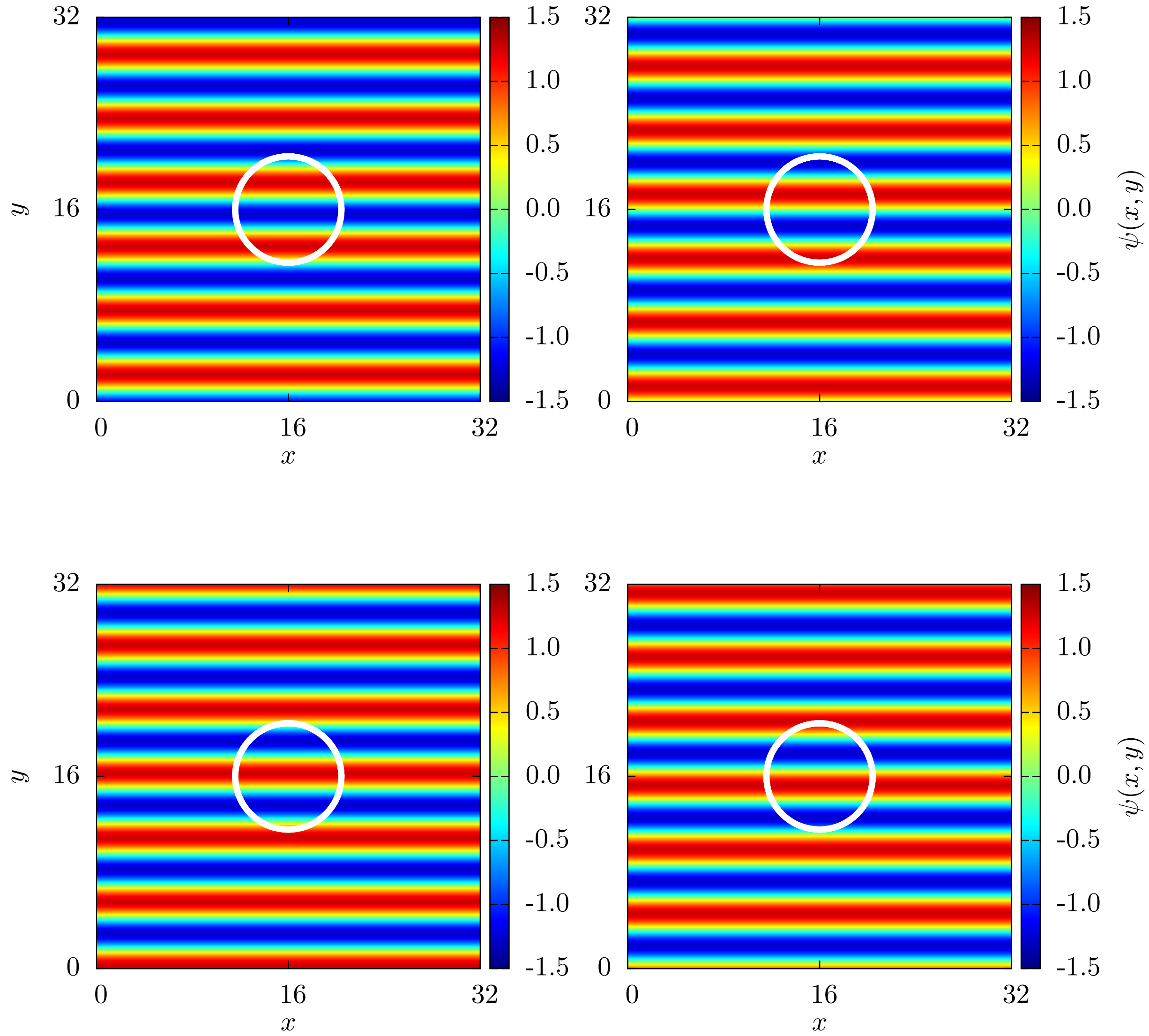

Figure 4.13: Snapshot of a drift bifurcation of Eckhaus unstable stripes. The white circle is a reference point, which allows to identify the movement to the bottom. Parameters are: $\epsilon = 1$, $\delta = 0$, $\alpha = 0.6$, $\tau = 2$, start with $\sin(1.178x)$, TDF turned on at $T = 0$.

5 Summary and Outlook

In this thesis, we analyzed the linear stability properties of general systems subjected to linear time delayed feedback. In particular, we considered TDF with scalar coupling matrices $\underline{\underline{K}} = \alpha \cdot \underline{\underline{1}}$, and derived the characteristic equation which determines the eigenvalues λ_j of the linear stability problem with TDF. We showed that the characteristic equation can be solved in terms of Lambert–W functions, and characterized properties of the solution. It was observed that every eigenvalue μ_j of the uncontrolled system state induces an infinite number of complex eigenvalues $\lambda_j(n)$, $n \in \mathbb{Z}$ of the linear stability problem with TDF, all of which satisfy the same characteristic equation.

Furthermore, we derived neutral stability curves which specify for which delay strength α and delay times τ a given eigenmode $\boldsymbol{\varphi}_j$ changes stability, and analyzed the implications for eigenvalues $\mu_j \in \mathbb{R}$ of the uncontrolled system state. It was shown that with the linear TDF control mechanism with scalar coupling matrices $\underline{\underline{K}} = \alpha \cdot \underline{\underline{1}}$, eigenvalues $\mu_j \in \mathbb{R}$ can be destabilized, but not stabilized. The analysis for $\mu_j \in \mathbb{C}$ is yet to be done, which presumably can be obtained by a generalization of the methods so far.

The analysis of TDF with scalar coupling matrices was then generalized to a certain subclass of non–scalar coupling matrices $\underline{\underline{K}}$, namely these in which the non–scalar coupling matrix commutates with the linearized operator $\underline{\underline{F'}}$ of F. Here, F denotes the non–linear operator that describes the intrinsic system dynamics of the uncontrolled system.

To confirm our analytical predictions and also to study the influence of TDF on a particular system, we considered the Swift–Hohenberg equation with TDF. We analyzed the TDF–induced instability of the homogeneous steady state, stripes and hexagons from the theoretical point of view. To this end, we derived and analyzed the order parameter equations for stripes and hexagons in the presence of TDF. It was demonstrated that the homogeneous steady state loses stability in a traveling wave bifurcation, whereas stripes and hexagons lose stability via a drift bifurcation, followed by a traveling wave bifurcation for larger values of α and τ. Comparing our analytical predictions with direct numerical simulations (DNS) showed good agreement.

Although all obtained numerical solutions so far lose stability at the expected bifurcation curves, the explanation of some of the resulting dynamical behaviour was out of the scope of our current analysis, such as a drift of Eckhaus unstable stripes or drifting ZigZag patterns. For instance, we observed stripes being destabilized by TDF and resulting in a drift of a ZigZag pattern, although the same scenario would not create a Zigzag instability in the system without TDF. Also, in the presence of TDF, we observed a drift bifurcation of stripes which would be Eckhaus unstable in the Swift–Hohenberg equation without TDF. Therefore, we conclude that TDF influences the boundaries of these so–called second instabilities of stripes (so–called Benjamin–Feir instability), which provides a good starting point for further analysis.

Bibliography

[ABR99] F Tito Arecchi, Stefano Boccaletti, and PierLuigi Ramazza. Pattern formation and competition in nonlinear optics. *Physics Reports*, 318(1):1–83, 1999.

[Bes06] Michael Bestehorn. *Hydrodynamik und Strukturbildung: Mit einer kurzen Einführung in die Kontinuumsmechanik*. Springer, 2006.

[Boy13] John P. Boyd. *Chebyshev and Fourier Spectral Methods: Second Revised Edition*. Dover Books on Mathematics. Dover Publications, 2013.

[BPA00] Eberhard Bodenschatz, Werner Pesch, and Guenter Ahlers. Recent developments in Rayleigh-Bénard convection. *Annual review of fluid mechanics*, 32(1):709–778, 2000.

[CGH+96] Robert M Corless, Gaston H Gonnet, D EG Hare, David J Jeffrey, and Donald E Knuth. On the Lambert w function. *Advances in Computational Mathematics*, 5(1):329–359, 1996.

[CH93] Mark C Cross and Pierre C Hohenberg. Pattern formation outside of equilibrium. *Reviews of modern physics*, 65(3):851, 1993.

[Gur13] Svetlana V. Gurevich. Dynamics of localized structures in reaction-diffusion systems induced by delayed feedback. *Phys. Rev. E*, 87:052922, May 2013.

[Gur14] Svetlana V Gurevich. Time-delayed feedback control of breathing localized structures in a three-component reaction-diffusion system. *arXiv preprint arXiv:1402.0985*, 2014.

[Hal93] Jack K Hale. *Introduction to functional differential equations*, volume 99. Springer, 1993.

[ITSO13] Ryosuke Iri, Yousuke Tonosaki, Kyohei Shitara, and Takao Ohta. Dynamics of turing pattern under time-delayed feedback. *Journal of the Physical Society of Japan*, 83(2), 2013.

[JBvL04] Wolfram Just, Hartmut Benner, and Clemens von Loewenich. On global properties of time-delayed feedback control: weakly nonlinear analysis. *Physica D: Nonlinear Phenomena*, 199(1):33–44, 2004.

[KBHS09] YN Kyrychko, KB Blyuss, SJ Hogan, and E Schöll. Control of spatiotemporal patterns in the gray–scott model. *Chaos: An Interdisciplinary Journal of Nonlinear Science*, 19(4):043126, 2009.

[LH07] Qian Shu Li and Hai Xiang Hu. Pattern transitions induced by delay feedback. *The Journal of chemical physics*, 127(15):154510, 2007.

[LM99] J. Lega and N. H. Mendelson. Control-parameter-dependent swift-hohenberg equation as a model for bioconvection patterns. *Phys. Rev. E*, 59:6267–6274, Jun 1999.

[LMN94] J Lega, JV Moloney, and AC Newell. Swift-Hohenberg equation for lasers. *Physical review letters*, 73:2978–2981, 1994.

[LWP01] O Lüthje, S Wolff, and G Pfister. Control of chaotic Taylor-Couette flow with time-delayed feedback. *Physical review letters*, 86(9):1745–1748, 2001.

[MS06] Alexander S. Mikhailov and Kenneth Showalter. Control of waves, patterns and turbulence in chemical systems. *Physics Reports*, 425(2â3):79 – 194, 2006.

[Mur93] James D Murray. *Mathematical Biology.* Springer, 1993.

[PVG+13] A Pimenov, AG Vladimirov, SV Gurevich, K Panajotov, G Huyet, and M Tlidi. Delayed feedback control of self-mobile cavity solitons. *Physical Review A*, 88(5):053830, 2013.

[Pyr92] K. Pyragas. Continuous control of chaos by self-controlling feedback. *Physics Letters A*, 170(6):421 – 428, 1992.

[SAJ+03] J Schlesner, A Amann, NB Janson, W Just, and E Schöll. Self-stabilization of high-frequency oscillations in semiconductor superlattices by time-delay autosynchronization. *Physical Review E*, 68(6):066208, 2003.

[Seg69] Lee A Segel. Distant side-walls cause slow amplitude modulation of cellular convection. *Journal of Fluid Mechanics*, 38(01):203–224, 1969.

[SH77] J Swift and Pierre C Hohenberg. Hydrodynamic fluctuations at the convective instability. *Physical Review A*, 15(1):319, 1977.

[SK09] Hans Rudolf Schwarz and Norbert Köckler. *Numerische Mathematik.* Springer DE, 2009.

[SS08] Eckehard Schöll and Heinz Georg Schuster. *Handbook of chaos control.* John Wiley & Sons, 2008.

[SSD09] Felix M Schneider, Eckehard Schöll, and Markus A Dahlem. Controlling the onset of traveling pulses in excitable media by nonlocal spatial coupling and time-delayed feedback. *Chaos: An Interdisciplinary Journal of Nonlinear Science*, 19(1):015110, 2009.

[SSM98] K. Staliunas and VÃctor J. SÃ¡nchez-Morcillo. Dynamics of phase domains in the Swift-Hohenberg equation. *Physics Letters A*, 241(1â2):28 – 34, 1998.

[TVPT09] Mustapha Tlidi, AG Vladimirov, Didier Pieroux, and D Turaev. Spontaneous motion of cavity solitons induced by a delayed feedback. *Physical review letters*, 103(10):103904, 2009.

[TVT+10] Mustapha Tlidi, AG Vladimirov, D Turaev, Gregory Kozyreff, Didier Pieroux, and Thomas Erneux. Spontaneous motion of localized structures and localized patterns induced by delayed feedback. *The European Physical Journal D*, 59(1):59–65, 2010.

[TZ13] Canrong Tian and Lai Zhang. Delay-driven irregular spatiotemporal patterns in a plankton system. *Physical Review E*, 88(1):012713, 2013.

[UAJS03] J Unkelbach, A Amann, W Just, and E Schöll. Time-delay autosynchronization of the spatiotemporal dynamics in resonant tunneling diodes. *Physical Review E*, 68(2):026204, 2003.

[vHMSZ01] J. von Hardenberg, E. Meron, M. Shachak, and Y. Zarmi. Diversity of vegetation patterns and desertification. *Phys. Rev. Lett.*, 87:198101, Oct 2001.

Danksagung

Zum Ende dieser Masterarbeit möchte ich mich bei folgenden Personen bedanken:

- Herrn Prof. Dr. Rudolf Friedrich für die vermittelte Begeisterung für die Forschung und die Möglichkeit diese Fragestellung in der Arbeitsgruppe bearbeiten zu können. Leider konnte er das Ende dieser Arbeit nicht miterleben.
- Herrn Prof. Dr. Stefan Linz für die zwischenzeitliche und Herrn Prof. Dr. Uwe Thiele für die letztendliche Übernahme der Betreuung und Begutachtung dieser Arbeit.
- Frau Dr. Svetlana Gurevich für ihre erstklassige Betreuung, interessante fachliche Diskussionen und für das Korrekturlesen dieser Arbeit.
- Herrn Markus Wilczek für seine Hilfsbereitschaft bei Fragen und Problemen aller Art, sowie für das Korrekturlesen dieser Arbeit.
- Meinen Bürokollegen Felix Tabbert und Walter Tewes für eine angenehme Atmosphäre im Büro.
- Meinen Korrekturlesern Simon Hannibal, Walter Tewes, Katrin Schmietendorf und Dorothea Mattner für ihren Einsatz gegen Fehler und das Kürzen überlanger Sätze.
- Der gesamten Arbeitsgruppe für nette und unterhaltsame Mittagessen und als Ansprechpartner bei Fragen.
- Meiner Familie für ihre Unterstützung beim Studium und in allen Lebenslagen.

Erklärung zur Masterarbeit

Hiermit versichere ich, Alexander Kraft, dass ich diese Arbeit selbstständig verfasst habe und dass außer den ausgewiesenen Hilfsmitteln und Quellen keine weiteren verwendet wurden. Zitate habe ich kenntlich gemacht.

Münster, den 01.05.2014